

## Review

### Interdiffusion in Group IV Semiconductor Material Systems: Applications, Methods and Discoveries

**Guangrui (Maggie) Xia**

Department of Materials Engineering, University of British Columbia, 309-6350 Stores Rd, Vancouver, BC V6T 1Z4, Canada

#### Contents

Abstract.....	2
1 Introduction and Background .....	3
1.1. The significance and necessity of interdiffusion research of group IV systems .....	3
1.2 Basic properties.....	5
1.3 Applications.....	6
1.3.1 SiGe and GeSn in FETs.....	6
1.3.2 SiGe:C in HBTs .....	7
1.3.3 Ge and GeSn for Si compatible lasers .....	8
1.3.4 Ge and GeSn as photodetectors and waveguides .....	10
2. Research Approaches in Interdiffusion Studies and the Benchmarking Si-Ge Interdiffusivity.....	10
2.1 Background of Si-Ge interdiffusion study and practical considerations.....	11
2.2 XRD approach.....	12
2.3 SIMS approach .....	13
2.4 The self-diffusivity approach.....	15
2.4.1 The theories in the self-diffusivity approach .....	15
2.4.2 Si and Ge self-diffusivity data.....	16
2.4.3 Interdiffusivity calculations .....	17
2.4.4 The benchmarking interdiffusivity .....	18
3. Impacting Factors of Interdiffusion: Stress, Doping, Defect Engineering and Threading Dislocation Density .....	21
3.1 Background and terms.....	21

3.2 Summary of major findings.....	21
3.3 Biaxial strain impacts .....	22
3.3.1 Biaxial strain impact on the driving force of interdiffusion .....	23
3.3.2 Biaxial strain impact on the interdiffusivity .....	24
3.4 Doping impacts .....	26
3.5 Defect impacts .....	31
4 Summary and prospective .....	32
5 Conflict of interest .....	33
6 Acknowledgements.....	33
References .....	34

## Abstract

Group IV semiconductor alloys, heterostructures and solid solutions such as SiGe, GeSn, Ge/Si and SiGe:C have been widely used and under extensive research for applications in major microelectronic and photonic devices. In the growth and processing of these materials, nanometer scale interdiffusion happens that are generally undesirable for device performance. With higher Ge molar fractions and higher compressive strains, Si-Ge interdiffusion can be much faster than dopant diffusion. However, Si-Ge interdiffusion behaviors have not been well understood until recent years. Much less studies are available for GeSn. This review starts with basic properties and the applications of major group IV semiconductors, and then reviews the progress made so far on Si-Ge and Ge-Sn interdiffusion behaviors. Theories, experimental methods, design and practical considerations are discussed together with the key findings in this field.

## 1 Introduction and Background

In the periodic table of elements, non-synthetic group IV elements include carbon (C), silicon (Si), germanium (Ge), tin (Sn) and lead (Pb). Among these elements, Si and Ge are the two most important elemental semiconductors. Specifically, Si has played a dominant and unreplaceable role in the semiconductor industry, which has revolutionized the world by enabling the Information Era. According to the product breakdown statistic data by World Semiconductor Trade Statistics (WSTS) 2017 report, Si-based semiconductor products including integrated circuits (ICs) and discrete components have occupied about 90% of the worldwide semiconductor market [1]. Today, the infrastructure, processing and analytical techniques and equipment used in the semiconductor industry are highly centered for Si-based products.

Besides the elemental semiconductors, group IV elements form a wide range of important semiconductors, and have wide applications in metal oxide semiconductor field effect transistors (MOSFETs), heterojunction bipolar transistors (HBTs) and photonic devices (Figure 1). They are in the forms of alloys (SiGe, GeSn, SiGeSn, GeC), compounds (SiC) and solid-state solutions (Si:C and SiGe:C). Incorporation of C in Si, SiGe and Ge can surpass the equilibrium solid solubility limits in temperature ranges relevant to technology and operation, but are commonly below 2 atomic percent without the formation of a second phase. The term “ $\text{Si}_{1-x}\text{C}_x$  alloy” or “Si:C solid-state solution” are both used. The latter one is used in this paper to avoid possible confusions with silicon carbide. SiC is a wide-bandgap semiconductor for power applications. Carbon allotropes such as graphene and carbon nanotubes are also interesting materials for electronic applications. This paper focuses on group IV semiconductors important for microelectronic and photonic applications, such as Si, SiGe, SiGe:C, Ge and GeSn.

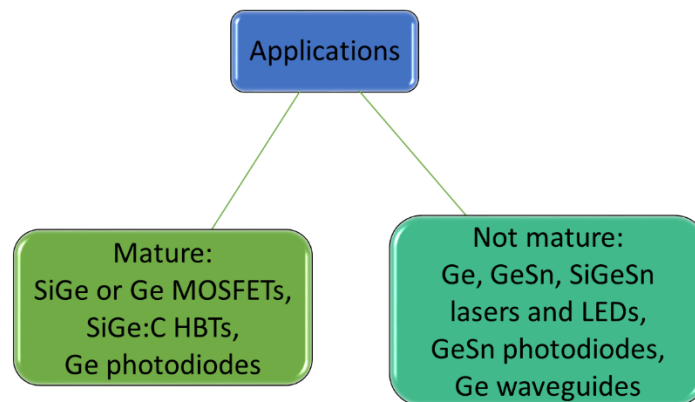


Figure 1. Major device applications of SiGe, Ge, GeSn, SiGeSn and SiGe:C.

### 1.1. The significance and necessity of interdiffusion research of group IV systems

Despite similar material properties, SiGe, SiGe:C, Ge and GeSn are still different material systems than Si. For example, the lattice mismatch between Ge and Si causes direct growth of high quality epitaxial Ge on Si difficult. Strain relaxation in lattice mismatched  $\text{Si}_{1-x}\text{Ge}_x/\text{Si}_{1-y}\text{Ge}_y$  and  $\text{Ge}_{1-x}\text{Sn}_x/\text{Ge}_{1-y}\text{Sn}_y$  epitaxial structures happens by misfit dislocations when the strained film thickness

is over the critical thickness. The thermal expansion coefficient of Ge is about twice of that of Si, which introduces thermal stress upon cooling and heating. The epitaxial growth, defect formation, lattice-mismatch stress, thermal stress and stress relaxation are all important considerations in the device processing, which have been studied intensively.

In high-end semiconductor devices, such as MOSFETs, bipolar transistors, lasers, high efficiency solar cells, single crystalline semiconductors are commonly doped with at least one dopant element. During the growth and processing of the semiconductor materials, high temperature steps, such as oxidation, source/drain anneal and deposition, are unavoidable. From a mass transport point of view, when a host matrix changes from Si to SiGe or to SiGe:C, or even with a change in stress/strain, dopant diffusion changes. On top of that, dopants segregate at  $A_{1-x}B_x/A_{1-y}B_y$  interfaces or with a gradual change in the composition. Si-Ge and Ge-Sn interdiffusion change the chemical concentration distributions directly, which impact the bandgap alignment, carrier transport, diffusion and segregation behaviors. For example, Si-Ge interdiffusion is generally undesirable as shape concentration differences are desired for quantum confinement or strain introduction. These three phenomena are significant topics for device structure design and materials processing, as dopant and alloy element distributions are critical factors in determining device characteristics and performance.

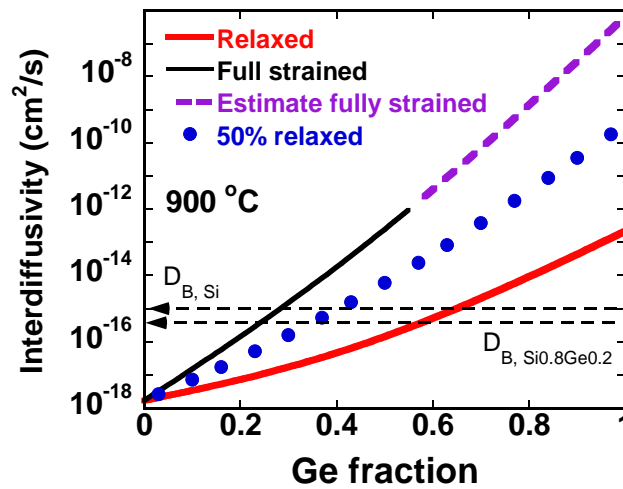


Figure 2. Si-Ge interdiffusivity at 900 °C for the whole Ge fraction range in comparison with boron (B) diffusivity in Si and  $\text{Si}_{0.8}\text{Ge}_{0.2}$ . The term “strained” and “relaxed” refer to the SiGe strain status on a relaxed Si substrate. Due to the very thin critical thickness (a few nanometer and below), fully strained high-Ge alloys coherent to a relaxed Si are not common, and are denoted with a dashed line.

It is interesting to compare dopant diffusivity and the interdiffusivity. Previously, Si-Ge interdiffusion was not as important as dopant diffusion, due to the much lower interdiffusivity in SiGe with lower Ge contents and lower compressive strain. It can be seen that when  $x_{\text{Ge}}$  is around 0.3, the interdiffusion in fully compressively strained SiGe is close to the B diffusivity, which is relevant to npn HBT application. In pMOS application, the source/drain stressors are boron doped, and are normally partially strained. Assuming 50% of the compressive strain is relaxed, when  $x_{\text{Ge}}$  is around 0.5, the interdiffusivity will be faster than the B diffusivity in Si and in  $\text{Si}_{0.8}\text{Ge}_{0.2}$ .

The reason that Si-Ge interdiffusion is not so obvious lies in the fact that Ge is a neutral alloy constitution instead of a donor or an acceptor element. Therefore, we consider interdiffusion and dopant diffusion with different scales. In considering the interdiffusion of Ge profiles, we commonly use a linear scale. For example, in HBTs, one atomic percent (1 at.%) Ge peak drop is common after thermal activation, which is a concentration change of  $5 \times 10^{20} \text{ cm}^{-3}$ . This is considered as a small change. While for dopant diffusion, we consider a change of  $1 \times 10^{19} \text{ cm}^{-3}$  quite significant.

Interdiffusion degrades MOSFET performance by reducing strain and carrier confinement and increasing alloy scattering [2, 3]. In HBTs, the change of Ge distribution impacts the band engineering and material properties, which needs to be carefully designed and closely monitored. For both MOSFET and HBT industry, higher and higher Ge contents are being used. For Ge-based photonic devices, interdiffusion changes Ge to SiGe alloys, which is more indirect bandgap than Ge, which is not desired. It decreases photodetector efficiency [4], reduces the direct band transitions and photoluminescence intensity, which delays the lasing of Ge/Si lasers [5].

This review starts with basic properties and the applications of major group IV semiconductors, and then reviews the progress made so far on Si-Ge and Ge-Sn interdiffusion behavior. Theories, experimental methods, design and practical considerations will be discussed together with the key findings in this field.

## 1.2 Basic properties

Ge is the most Si-compatible semiconductor because it has the same crystalline structure (diamond cubic structure), close lattice constants (a 4.18% larger lattice constant) and similar properties such as energy band structure, stiffness constants, Poisson ratio, self-diffusivity, and specific heat. Ge and Si are miscible in the full concentration range. They are both indirect bandgap semiconductors. At 300 K, the indirect bandgap energy of Si is 1.12 eV. The direct and indirect bandgap energies of Ge are 0.80 eV and 0.66 eV respectively at 300 K. Ge can be engineered to become a pseudo-direct or direct bandgap semiconductor by the introduction of tensile strains and/or n-type doping [6]. Tensile strains lower Ge's direct energy bandgap energy faster than the indirect bandgap energy. Large enough tensile strain (biaxial tensile strains  $> 1.8\%$  or uniaxial tensile strains  $> 4.6\%$ ) can convert Ge to a true direct-bandgap semiconductor without any doping [7].

Similarly, the energy band structures of  $\text{Ge}_{1-x}\text{Sn}_x$  alloys can be engineered by the Sn content. Low Sn content GeSn alloys are of particular interests for applications in MOSFETs due to their high hole mobilities. They can also be made as light emitting diodes, photodetectors and lasers due to the direct bandgap suitable for mid-infra-red absorption and emission. The introduction of Sn can lower Ge's direct energy bandgap faster than the indirect bandgap. Based on experiments and their extrapolation, the indirect to direct band transition of  $\text{Ge}_{1-x}\text{Sn}_x$  is at around  $x = 0.09$  for relaxed  $\text{Ge}_{1-x}\text{Sn}_x$ . On the solubility aspect, Ge and Sn form a binary eutectic alloy, with the eutectic temperature of 231.1 °C. The thermal equilibrium solid solubility of Sn in the Ge matrix is as low as 1 at.% below 500 °C [8]. As a result, it is difficult to increase the Sn content in  $\text{Ge}_{1-x}\text{Sn}_x$  alloys because Sn precipitates from solid  $\text{Ge}_{1-x}\text{Sn}_x$  easily during the crystal growth and post-growth

processes. In recent years, Sn incorporation above the solid solubility has been achieved using chemical vapour deposition (CVD), molecular beam epitaxy (MBE) and solid state-epitaxy methods.

Less than 0.5 atomic percent carbon in Si or SiGe is mainly used in SiGe HBTs for its capability in defect and thus diffusion and junction engineering. The current understanding is that carbon diffuses via an interstitial mechanism, thus reducing the concentration of Si self-interstitials [9-11]. This in turn retards the diffusion of interstitial diffusers such as boron in Si and  $\text{Si}_{1-x}\text{Ge}_x$  ( $x < 0.2$ ) and phosphorus in Si. This approach is especially useful for NPN SiGe HBTs, which has been utilized in the industry since late 80's. The carbon incorporation approach is less effective for phosphorus in PNP SiGe HBTs, due to the small percentage of vacancy-assisted diffusion for P in  $\text{Si}_{1-x}\text{Ge}_x$  ( $x < 0.18$ ).

### 1.3 Applications

In the past three decades, due to the compatibility with the mainstream Si processing and the capability of energy bandgap/band structure, mobility, strain, and diffusion engineering, SiGe, SiGe:C, and Ge have been commercially and widely used in electronic and optoelectronic devices (Figure 1) such as MOSFETs [12-15], tunnel field-effect transistors (TFETs) [16, 17], SiGe:C, hetero-junction bipolar transistors (HBTs) [18-21], photodetectors [22-24], modulators [25-27], and waveguides [28-30]. Besides these industry applications, many SiGe devices have been under extensive research such as SiGe nanowires transistors [31], Si and Ge nanocrystals thin film transistors and light emitters [32, 33], Ge quantum dots lasers [34], Ge quantum dot photodetector [35], GeSn lasers [34, 36-38] and Ge lasers [39], SiGeSn light emitting diodes (LEDs) [36] and photodetectors [40, 41].

The advantages of using SiGe, Ge, Si:C, GeSn are multifold. First, as discussed above, SiGe, Ge and GeSn have higher hole mobility than Si, which can be used as high hole mobility channel materials to boost MOSFET performance. Secondly, the lattice-mismatch can be used to introduce tensile or compressive strain, which changes energy band structures and carrier mobilities as well. These two approaches can be combined together. Tensile strain can increase electron mobility while compressive strain are good for hole mobility. Si:C can serve as tensile stressors for Si and SiGe channels. SiGe and GeSn can serve as compressive stressors for SiGe or Ge channels with smaller lattice constants. Thirdly, these materials can be used to engineer the bandgap structures such as the case for SiGe HBTs and SiGe TFETs. Fourthly, carbon is used to reduce interstitial concentrations and retard interstitial diffuser such as B in Si and in SiGe. Overall, the addition of other elements give more dimensions in engineering the material properties of the host material.

#### 1.3.1 SiGe and GeSn in FETs

Si-based MOSFETs have been the most important and widely used semiconductor transistors, which are the fundamental building blocks of digital ICs. Since the 90 nm node production in 2004, SiGe has been used commercially in the state-of-the-art digital integrated circuits as source and drain stressors in p-type MOSFETs to introduce compressive stress to the channels and enhance hole mobility until the 10 nm node FinFETs technologies. In a 2018 report by MSSCORPS Corporation Ltd., cross-section electron microscopy (XTEM) images and energy dispersive X-ray

spectroscopy (EDS) mapping images of two cell processors, Exynos8895 and A11 Bionic used in Samsung’s Galaxy S8 and iPhone 8 respectively, are shown. The two processors both used 10 nm node technologies, which were fabricated by Samsung and Taiwan Semiconductor Manufacturing Company (TSMC) respectively. SiGe stressors for pMOSFETs are clearly seen in these images. SiGe-channel FinFETs with 25% Ge were used as 10 nm node pFET channels [42]. The benefits include better current drive and reliability [42]. 40% Ge channel FinFETs were reported in 2017 and shown in Figure 2 (a) and (b) [43].

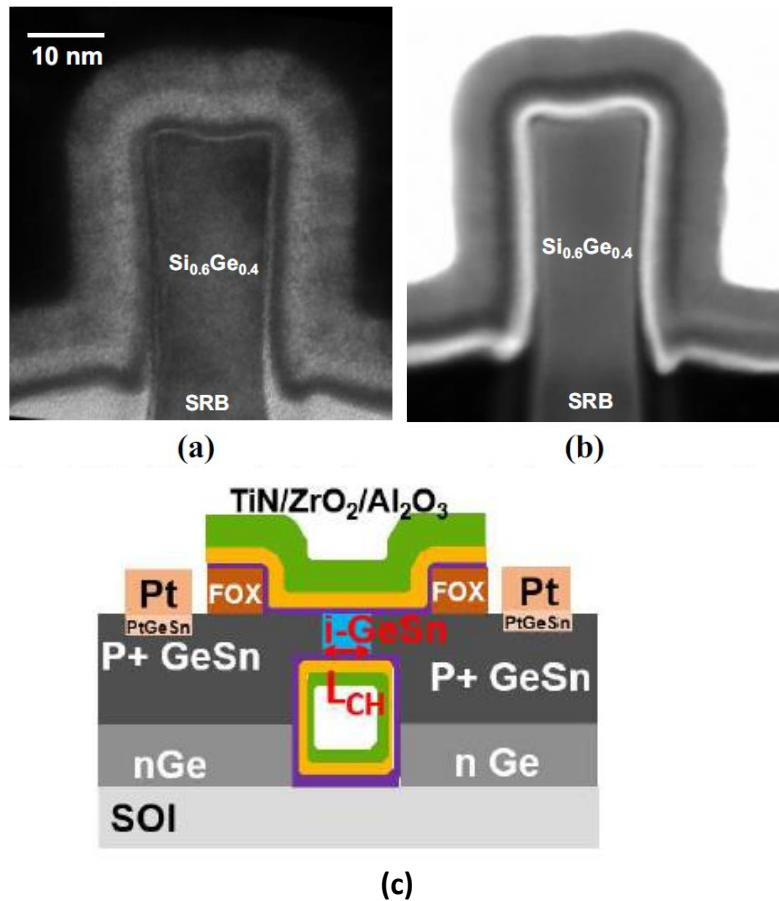


Figure 2 (a) Transmission electron microscopy (TEM) image, and (b) a high-angle annular dark-field imaging (HAADF) of compressively-strained  $\text{Si}_{0.6}\text{Ge}_{0.4}$  pFinFETs on a strained relaxed buffer (SRB). (c) Schematic cross-sectional view of single-GeSn channel. Figure reproduced from [43, 44] with permission from IEEE.

There are various GeSn electronic device applications, such as high mobility channel MOSFETs with  $\text{Ge}_{1-x}\text{Sn}_x$  source and drain stressors [45], high-mobility  $\text{Ge}_{1-x}\text{Sn}_x$  channel MOSFETs with up to 10% Sn as in Figure 2 (c) [44] and tunnel field-effect transistors (TFETs) [46] for high-performance and low-power consumption devices.

### 1.3.2 SiGe:C in HBTs

HBTs were dominated by III-V compound semiconductors before the emergence of SiGe HBTs, which were enabled by the lattice-matched strained-SiGe epitaxy technology. The use of SiGe:C

in HBTs can be dated back to the late 80's, when it was first demonstrated by IBM [18]. SiGe is used to form a base with a narrower bandgap. Ge composition is typically graded across the base to create an accelerating electric field to help minority carriers to move faster across the base. A peak Ge molar fraction of 20% is commonly used with 20 to 30% Ge in R&D.

For HBTs in high-speed and high-frequency applications, there are two important figures-of-merit, which are the common-emitter short-circuit cut-off frequency  $f_T$  and the maximum frequency of oscillation  $f_{max}$ . Higher  $f_T$  and  $f_{max}$  represent better HBT device performance. Reducing the base width is an effective way to reduce the base transit time and thus increase  $f_T$ . Physically, higher base doping reduces electrical resistance, while narrower base doping profile reduces carrier transit time in the base region. These all contribute to a higher  $f_T/f_{max}$ . Heinemann et al. recently reported experimental results of  $f_T/f_{max}$  for up to 505/720 GHz [47]. Aggressively scaled base doping profiles and the use of advanced annealing techniques are among the most important approaches to improve  $f_T/f_{max}$ . Carbon incorporation is one of the most important approaches to control B diffusion in NPN SiGe HBTs, creating narrower bases. The mechanism lies in the fact that C reduces interstitial concentration, which in turn reduces B diffusivity in Si and SiGe as B diffuses 100% by interstitials [48]. Carbon molar fractions used are generally from 0.1 to 0.3%. In SiGe:C systems, carbon is normally treated as an impurity instead of an alloy component. The major purpose of carbon incorporation is for point defect engineering, and due to the small concentration of carbon and the low solubility in SiGe, the focus of carbon in SiGe is on its substitutional portion and

For SiGe NPN HBTs and PNP HBTs, the base layers are commonly a few nm wide inside triangle-shaped Ge profiles. The main stream annealing is done by rapid thermal annealing (RTA) with a peak temperature in 1000 to 1100 °C range. Changes in Ge profiles now is about 1-3 % at the triangle tip part of Ge profiles. With the scaling in width, the increase in the Ge concentration to 25 to 30% and thus the increase of compressive strain, more changes in Ge profiles due to interdiffusion are expected, which has a big impact in the energy band engineering, the processing condition design and the performance of SiGe HBTs.

### 1.3.3 Ge and GeSn for Si compatible lasers

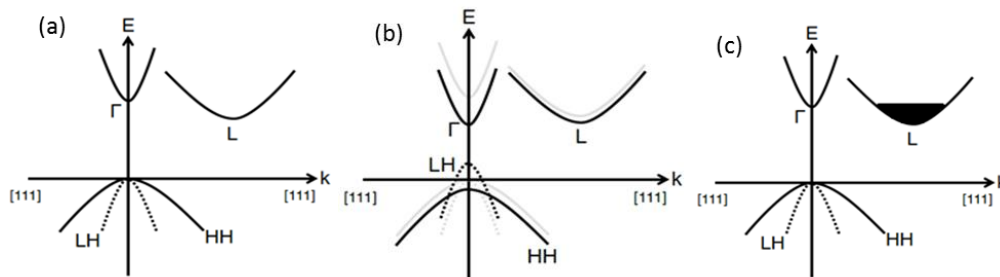


Figure 4. Schematic diagrams of band structures of Ge under different conditions. (a) Ge without strain or doping; (b) tensile strained Ge without doping; and (c) highly n-type doped Ge without strain. Figure reproduced from [6], an open access paper by OSA Publishing.



Ge and GeSn have also been studied for Si-compatible lasers [49-55] in the past two decades. The major motivation to study group IV lasers is their material and processing compatibility with the Si manufacturing infrastructure. Another important factor is in that Ge can be engineered into a pseudo-direct bandgap or direct bandgap semiconductor by adding tensile stresses or n-type doping or Sn as its direct bandgap is only 136 meV larger than its indirect bandgap.

In 2007, Jifeng Liu et al. from MIT showed that Ge can become a pseudo-direct bandgap material by adding tensile strain and/or high n-type doping as shown in Figure 4 [56]. The n-type doping is used to fill the bottom energy states of the L valley such that the energy of the remaining available states can be higher than the bottom of the  $\Gamma$  valley of the direct band. In 2010, an optically pumped Ge-on-Si laser was first realized by adding a 0.24% biaxial tensile strain [49]. It operated with a gain of  $50 \text{ cm}^{-1}$  at an n-type doping of  $1 \times 10^{19} \text{ cm}^{-3}$  at room temperature. The lasing wavelength range was from 1590 to 1610 nm. In 2012, an electrically pumped Ge-on-Si laser was first demonstrated by researchers from MIT and APIC Corporation. It worked at room temperature and had a phosphorus (P) doping level of  $4 \times 10^{19} \text{ cm}^{-3}$  and a 0.2% biaxial tensile strain, as shown in Figure 4 (c). The lasing wavelengths were from 1520 to 1700 nm due to different clamping conditions and the output power was up to 7 mW at room temperature [51]. The threshold current density was  $280 \text{ kW/cm}^2$ .

Tensile strains can be introduced by thermal expansion coefficients mismatch between Si substrates or by stress concentration methods. As shown in Figure 4 (b), with an additional tensile strain applied to Ge, the  $\Gamma$  valley in Ge shrinks faster than the L valleys due to the smaller effective mass in the  $\Gamma$  valley. For Ge to become a direct band gap material, according to calculations and experiments, the applied tensile strain need to be  $> 1.8\%$  for biaxial strain or  $> 4.6\%$  for uniaxial strain [7]. However, such high tensile strains narrow the bandgap too much so that the lasing wavelength will be larger than two microns [57]. Besides, it is technically hard to achieve such high tensile strain in Ge. There have been successful experimental efforts to change Ge into a direct bandgap material by introducing high uniaxial tensile strain up to 5.7% [57]. However, up to now, no successful efforts have been reported in making undoped Ge-on-Si lasers with tensile strain only.

Si-Ge interdiffusion has been shown to be mediated mostly by vacancies [58-60]. For Ge-on-Si lasers, due to an n-type doping introduced increase in vacancy concentrations, interdiffusion during annealing steps has been shown to be increased by 1 to 7 times for mid- $10^{18} \text{ cm}^{-3}$  P-doped Ge on Si [58, 61]. The defect annealing steps are commonly needed to reduce TDD for Ge epitaxy. In our recent work, photoluminescence (PL) intensity measured from n-doped Ge-on-Si after defect annealing is much reduced from that of unannealed samples, and more indirect band transitions are observed after annealing [5]. This shows the contradicting effects between the defect reduction and interdiffusion. Within the experiment conditions, the PL data suggested that the negative impact from interdiffusion is larger than the benefits from the defect annealing. Therefore, a defect annealing step may not be needed for n-doped Ge/Si.

GeSn lasers emerged after Ge-on-Si lasers. S. Wirth reported the first optically pumped GeSn laser in 2015 with 12.6% Sn [53]. The working temperatures were below 90 K, and the threshold

current density was 325 kW/cm<sup>2</sup>. Later reported GeSn lasers showed operations up to 130 K and the wavelengths were between 2 to 3.1 microns [54, 55].

### 1.3.4 Ge and GeSn as photodetectors and waveguides

As discussed above, Ge has an indirect bandgap 0.66 eV at room temperature, which corresponds to around 1.55 μm in wavelength. As a result, its optical applications are mainly in short infrared or mid-infrared region. Light detection and modulation can be realized with Ge-on-Si waveguides. Ge waveguide p-i-n photodetectors have achieved 67 Gb/s operation [62]. Ge-on-Si waveguides can work for 1.5486 μm wavelength [63] and larger wavelength, such as between 5.2 and 5.4 μm with a minimum propagation loss of 3 dB/cm [64]. A more recent experiment had operating wavelengths between 7.5 and 8.5 μm and a minimum propagation loss of 2.5 dB/cm at 7.575 μm wavelength [30].

The indirect and direct bandgap of Ge<sub>1-x</sub>Sn<sub>x</sub> alloys decreases with the Sn concentration. Therefore, the corresponding wavelengths are larger compared to Ge photodetectors and waveguides. The transition to a direct bandgap GeSn happens at around 8 at.% Sn for relaxed GeSn. Theoretically, the wavelength could be extended to 2.32, 2.69, and 4.06 μm for Ge<sub>0.97</sub>Sn<sub>0.03</sub>, Ge<sub>0.95</sub>Sn<sub>0.05</sub>, and Ge<sub>0.90</sub>Sn<sub>0.10</sub> waveguide photodetectors under 1% tensile strain respectively [36]. Photodetection up to 2.2 μm was achieved experimentally by Ge<sub>0.91</sub>Sn<sub>0.09</sub> quantum wells on silicon substrate [65]. Tseng et al. reported GeSn photodetectors with a larger photo-responsivity with only 2% Sn concentration. The operation speed can reach 6.2 GHz [66]. Quantum efficiency analysis indicated that Sn introduction can also reduce the device length to achieve the maximum efficiency about 60% at 1550 nm wavelength in waveguide photodetectors [67].

Preliminary GeSn lasers work at very low temperatures such as 90 to 130 K as discussed previously. Amplified spontaneous emission was observed by optically pumped GeSn waveguides at room temperature [68]. However, the net cavity gain could not exceed the lasing threshold in the experiment, which is a barrier for GeSn laser development [40].

Another important application for GeSn alloys is in light-emitting diodes (LED), which are more mature than GeSn lasers. GeSn LEDs with an indirect bandgap have been well studied at temperatures from 77 to 300 K with Sn concentrations up to 9.2% [69]. Direct bandgap GeSn LEDs have been demonstrated, which have Sn concentration up to 11% and the emitted phonon energy is 0.55 eV (wavelength = 2.25 μm) at room temperature [37].

## 2. Research Approaches in Interdiffusion Studies and the Benchmarking Si-Ge Interdiffusivity

For a binary system with element A and B, according to Darken's law in Equation (1), when the molar fraction of A is much less than that of B, it can be considered as a dilute solution of A in B.

$$\tilde{D} = D_A x_B + D_B (1 - x_A) \quad (1)$$

In these cases, the interdiffusivity is approximately the intrinsic diffusivity of A in B. The study of interdiffusivity is meaningful when the dilute solution condition doesn't apply, which depends on the difference between  $D_A$  and  $D_B$  and the accuracy needed.

The complications of binary semiconductor alloy systems lie in the concentration, strain, defect density, point defect engineering (such as carbon incorporation and oxidation) and doping, which are all technologically significant that impact the interdiffusion simultaneously. For example, Si-Ge interdiffusivity has a very strong dependence on the Ge concentration. For relaxed SiGe with low defect density and no intentional doping in the temperature range from 700 to 1000 °C, the interdiffusivity at the Ge end is 5 to 6 orders of magnitude larger than that at the Si end [70]. It increases exponentially with the compressive strain, and increases with n-type dopants and implant damage [2, 71-73].

To be relevant to the modern industry practice, atomic-scale interdiffusion studies require a great material quality, a careful experiment design to separate the impacting factors, and a high accuracy in the thermal annealing temperatures and characterization tools. Here are some key experimental considerations.

- 1) High quality epitaxial systems with low dislocation density (commonly below mid- $10^{16} \text{ cm}^{-3}$  and well-defined concentration profiles are required.
- 2) Strain status needs to be closely monitored such that interdiffusion can happen with a known strain history. This in turn requires a careful design of the film stacks and thermal budgets.
- 3) Temperature calibration is crucial to the accuracy of data and modeling. A temperature accuracy of a few degrees is required. Mainstream rapid thermal anneal (RTA) tools work by the thermal absorption of intense light emission. RTA tools are very sensitive to the chamber cleanness, and are much harder to calibrate for general purpose cleanrooms, where various materials are used. A practical solution is to use industry R&D facility where the annealing tools are well-maintained and calibrated for a narrow group of material systems. However, the industry tools are hard to get access to. Another option is to use a heating stage or a furnace with resistive heating.
- 4) Atomic scale Si and Ge depth profiling are normally done by secondary ion mass spectrometry (SIMS). Although SIMS tools are not rare in Canadian and US schools, we have not found any SIMS tools in an academic setting that is calibrated enough to cover the full Ge fraction ranges. For our studies at MIT and the University of British Columbia (UBC), SIMS measurements have been commercially performed by Evans Analytical Group, who provides good data repeatability and accuracy.

In the discussions below, we will mostly use the Si-Ge binary system as an example to discuss the methods used in interdiffusion studies.

## 2.1 Background of Si-Ge interdiffusion study and practical considerations

Major Si-Ge interdiffusion research efforts started in the 1990's. Several groups measured the interdiffusion with various techniques such as SIMS [74], Rutherford backscattering spectrometry [75, 76], X-ray diffraction (XRD) [77, 78], Raman spectroscopy [79] and photoluminescence [80]. Typical interdiffusion structures studied in the 90's were Si/Si<sub>1-x</sub>Ge<sub>x</sub> superlattices with thickness from 30 nm to a few microns and in low Ge ranges ( $x_{Ge} < 0.3$ ). Due to device scaling and advancement in structures and fabrication techniques, typical Si-Ge interdiffusion lengths in current technologies are in 1 to 100 nm range, comparable to the thickness of SiGe thin films in the devices.  $x_{Ge}$  range of current interest is now much higher than previous studies. Therefore, in the past one to two decades, Si-Ge interdiffusion has been revisited. Generally there are three major approaches to study SiGe interdiffusion experimentally.

## 2.2 XRD approach

The first approach uses high resolution X-ray diffraction (HRXRD) to probe multiple layered superlattice structures, which can also be considered as multiple quantum wells (MQWs), which was used by researchers such as Aubertine, Meduna, Ozguven and Liu *et al.* [81-85]. The principle underlying this technique is the correlation between the interdiffusivity and Bragg reflection intensity decay rate of superlattice satellite:

$$\frac{d}{dt} \left[ \frac{I(t)}{I(0)} \right] = - \frac{8\pi^2}{\lambda^2} \tilde{D}, \quad (2)$$

where  $I(t)$  is the superlattice satellite intensity measured by XRD as a function of the annealing time  $t$ ,  $\lambda$  is the spatial period of the superlattice, and  $\tilde{D}$  is the interdiffusivity.

This technique utilizes the ultrahigh sensitivity of XRD for concentration modulated films. However, this method only solves one interdiffusivity for one superlattice, which is an averaged interdiffusivity for a concentration range. As Aubertine *et al.* pointed out, when it was applied to concentration dependent interdiffusion like Si-Ge interdiffusion, this method is only suitable for superlattices Si<sub>1-x</sub>Ge<sub>x</sub>/Si<sub>1-y</sub>Ge<sub>y</sub> with a low amplitude [81]. This method also ignores the strain distribution in a superlattice, which has a tensile/compressive pattern, and the strong dependence of the interdiffusivity on  $x_{Ge}$ . The limitation of this method is that it is an indirect way of monitoring interdiffusion, compared to SIMS. For each Ge fraction studied, a superlattice structure with a narrow Ge fraction amplitude needs to be grown, which is normally not device-related structures. The advantage of this method is that XRD is a very sensitive non-destructive method, which can monitor the time evolution of interdiffusivity. It is suitable for a lab with a good epitaxy growth capability.

Aubertine *et al.*'s work focused on the interdiffusion in MQW with  $x_{Ge}$  below 0.2 and in a temperature range from 770 to 880 °C (Figure 5). The interdiffusion was modelled with a concentration-dependent diffusivity pre-factor  $D_0$  and activation energy  $E_a$ . Ozguven *et al.* measured the interdiffusivity at  $x_{Ge, average} = 0.91$  [82]. To avoid too much averaging over a large Ge range, the Ge molar fraction difference in each MQW is 0.05.

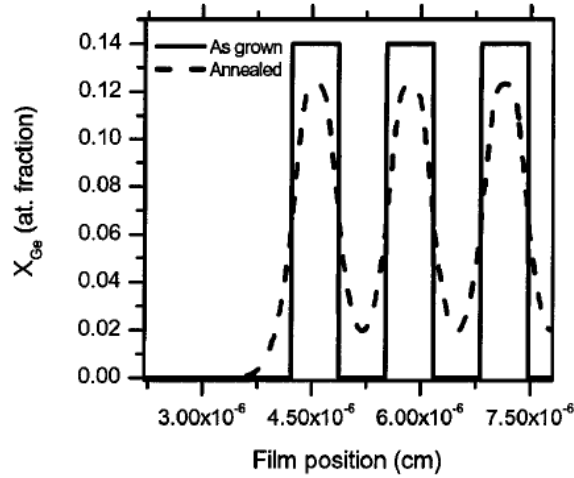


Figure 5. Assumed as-grown Ge molar fraction profile and annealed Ge profiles of a multiple quantum well structure. Figure reproduced from [81] with permission from AIP Publishing.

With much larger Ge molar fraction differences from 0.15 to 0.80 in one period of MQWs, Meduna *et al.* investigated four  $x_{Ge, average}$  (from 0.25 to 0.90) and obtained similar interdiffusivity formulas to Aubertine's [83, 84]. Liu *et al.* measured it at  $x_{Ge, average} = 0.85$  with a  $x_{Ge}$  difference of 0.35 in one period of MQWs [85]. There are two significant issues with large  $x_{Ge}$  differences in one period of MQWs. First, the  $x_{Ge}$  corresponding to the interdiffusivity is taken as the  $x_{Ge, average}$  of MQWs or measured by Rutherford backscattering spectrometry. This is not a good method to obtain the nominal Ge value as the interdiffusivity depends on  $x_{Ge}$  exponentially instead of linearly. According to the model reported by Gavelle *et al.*, for one period of  $Si_{0.45}Ge_{0.55}/Ge$  MQW, the interdiffusivity in the compressive Ge layer is almost 1000 times larger than that in the  $Si_{0.45}Ge_{0.55}$  layer [86]. Once the interdiffusion starts, Ge from the higher Ge regions diffuses out to the lower Ge molar fraction layer, which reduces the difference.

Recently, interdiffusion in a Ge-Sn system was studied using the XRD approach [36].  $Ge/Ge_{0.9}Sn_{0.1}$  MQW structures were used. The annealing temperatures studied were from 300 to 600 °C. For the temperature range from 380 to 450°C, the effective interdiffusivity is in the range of  $10^{-16}$  to  $10^{-15}$   $cm^2/s$ , where the Sn molar fraction  $x_{Sn}$  ranges from 0 to 0.1. They described the interdiffusivity using an Arrhenius relation.

$$\tilde{D}_{effective} = 2.9 \times 10^{-7} cm^2 s^{-1} \exp\left(-\frac{1.21eV}{kT}\right) \quad (3)$$

So far, this work has been the only experimental work that we are aware of on Ge-Sn interdiffusion. More detailed studies on Ge-Sn interdiffusion need to be performed.

### 2.3 SIMS approach

The other technique employs SIMS. Cowern *et al.*'s work in 1994 used SIMS to measure diffused Ge profiles, and used diffusion models to fit the profiles. Xia *et al.*'s work in 2006 and 2007 first introduced Boltzmann-Matano method to extract Si-Ge interdiffusivity  $\tilde{D}_{Si-Ge}$  as a function of  $x_{Ge}$  from the diffused profiles of step structures [71], as shown in Figure 6. (a). Boltzmann-Matano method can be used to extract the interdiffusivity from an annealed concentration

profile when the pre-diffusion profile can be approximated as a step profile, also known as an interdiffusion couple. This method also requires that the interdiffusivity is only dependent on the alloy concentration. This condition can be satisfied when an epitaxial system is pseudomorphic where the strain dependence can be expressed as a Ge concentration dependence and the annealing is isothermal with no significant change in the strain or the dislocation density. The isothermal condition the interdiffusion couple condition are easy to satisfy. However, other conditions are not easy to satisfy. For example, if there is strain relaxation or a non-uniform distribution of threading dislocations or doping, the interdiffusivity is no longer a pure function of the Ge concentration. These scenarios are common in the industry practice, in which cases, we can still use this method to estimate the interdiffusivity, which is then called the effective interdiffusivity.

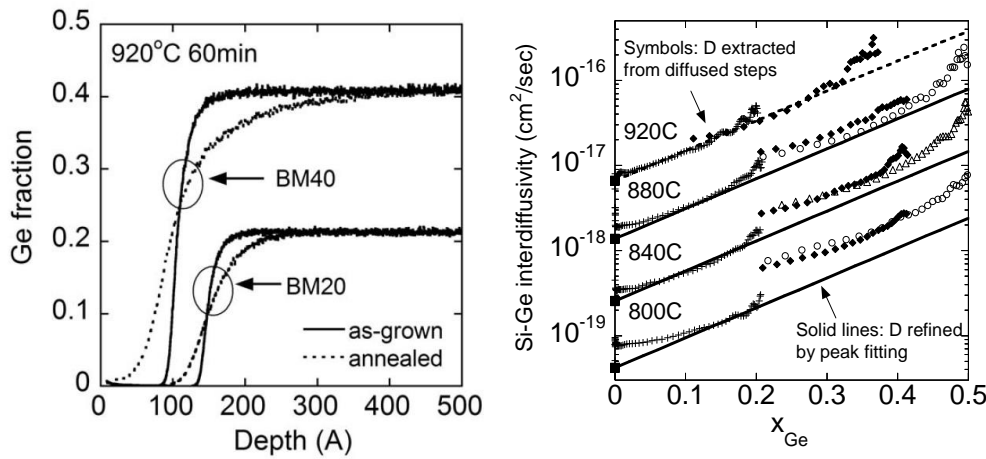


**Figure 6. (a) Ge profiles of the interdiffusion couples up to 40% Ge before and after diffusion. (b) Interdiffusivity extracted from Boltzmann-Matano analysis (symbols) compared to the  $D_R$  model expressed in Equation 1 (solid lines). Squares at  $x_{Ge} = 0$  are Ge tracer diffusivity data. Figure adapted from Ref. [71] with from AIP Publishing.**

Compared with the XRD approach, the SIMS and Boltzmann-Matano analysis approach makes it convenient to extract  $\tilde{D}$  as a function of  $x_{Ge}$ . It also works well to include the strain impact, as it can be expressed as a function of  $x_{Ge}$  in coherent epitaxial films. The step structures are easier to grow than superlattice structures. Most importantly, the diffusion structures are device-relevant.

Using this approach, Xia *et al.* built a  $D_R D_C$  model to describe the Si-Ge interdiffusivity under relaxed, tensile and compressive stress (Figure 6) [71]. This work reveals the exponential dependence of interdiffusivity on the Ge fraction and biaxial compressive strain.

$$D_{R/T}(x_{Ge}) = 310 \exp\left(-\frac{4.66\text{eV}}{kT}\right) \exp(8.1 * x_{Ge}), \quad (4)$$

$$D_C(x_{Ge}) = D_R(x_{Ge}) * \exp\left(s * \frac{|\epsilon_c|}{0.042}\right), \quad (5)$$

where  $s \approx 15$ ,  $D_{R/T}$  refers to interdiffusivity under relaxed or tensile strain, and  $D_C$  refers to that under compressive strain. All strains here are biaxial due to planar growth of thin epitaxial films.

The error bar of this model is from 50% to 150% of the measured diffusivity, which is mainly from annealing temperature uncertainty and SIMS errors. Although the  $D_{RD_C}$  model lacks a detailed theoretical study on the activation energy dependence, it catches the interdiffusion behavior (the Ge fraction, stress and temperature dependence) with quite reasonable accuracy and an easy to implement format. In 800 to 1200 °C, the temperature range relevant to technology, this model has been used to predict interdiffusion for both furnace anneals and RTAs, and has been shown to be reasonably accurate as seen in Dong *et al.*'s work [70]. Therefore, this model can be used as the first model to predict interdiffusion for  $x_{Ge} < 0.56$ .

With an amorphous Ge/Si structure, Si/Ge, Gavelle *et al.* extracted and then modelled experimental interdiffusivity with a two-term equation. One term was for dislocation-mediated interdiffusion, and the other for lattice mediated interdiffusion [86]. Due to the high dislocation density ( $10^{10} \text{ cm}^{-2}$ ) in their structures, Gavelle *et al.*'s data are good to show the dislocation-mediated interdiffusion term. In the high Ge region, the data agree with Dong *et al.*'s model quite well.

## 2.4 The self-diffusivity approach

Besides the two approaches discussed above, Dong *et al.*'s work at UBC first introduced the third approach in studying Si-Ge interdiffusivity under no stress or tensile stress, which is the self-diffusivity approach [70]. This approach is based on Si, Ge self-diffusivity and chemical activity coefficients. Interdiffusivity is calculated from these data instead of from direct measurement of interdiffusion. The advantage of this approach is that it is able to cover a wide range of temperature and Ge fraction range, and is especially useful for interdiffusion under rapid thermal annealing conditions, where temperature range is large. In addition, this interdiffusivity model provides a zero strain, no doping, and low dislocation density reference for later studies of more impacting factors of SiGe interdiffusion. To use this model for structures with compressive strains, a compressive strain enhancement factor, such as that in the  $D_{RD_C}$  model in Equation (5) or that in Equation (16) (discussed in section 3.3) need to be added to account for that.

Darken's law was first reported by L. S. Darken in 1948 for binary metallic systems [87]. It describes the correlation between self-diffusivity, intrinsic diffusivity and interdiffusivity under equilibrium point defects.

### 2.4.1 The theories in the self-diffusivity approach

From thermodynamics and basic diffusion theory, intrinsic diffusivity  $D$  can be expressed as:

$$D = MR_g T \left( \frac{\partial \ln a}{\partial \ln x_A} \right) \quad (6)$$

where  $M$ ,  $R_g$ ,  $T$ ,  $a$ , and  $x_A$  denote the mobility, the ideal gas constant, the absolute temperature, the chemical activity and the molar fraction of component A.



The term  $\frac{\partial \ln a}{\partial \ln x_A}$  counts for the chemical mixing effects. For ideal solutions, such as mixtures of different isotopes of one element,  $\frac{\partial \ln a}{\partial \ln x_A} = 1$ . The diffusivity of one isotope in chemically homogenous solutions is called self-diffusivity  $D^*$ , which is macroscopically expressed as  $D^* = MR_g T$ . In reality, semiconductors with low to medium doping levels are very close to ideal solutions. SiGe alloys, on the other hand, have comparable Si and Ge concentrations, and thus can't be treated as ideal solutions.

For non-ideal solutions,  $\frac{\partial \ln a}{\partial \ln x_A} \neq 1$ , and the influence from chemical mixing cannot be ignored. In these cases, the diffusivity  $D$  is intrinsic diffusivity. The relation of self-diffusivity and intrinsic diffusivity can be expressed as

$$D_A = D_A^* \left( \frac{\partial \ln a_A}{\partial \ln x_A} \right) = D_A^* \left( 1 + \frac{\partial \ln \gamma_A}{\partial \ln x_A} \right), \quad (7)$$

where  $\gamma_A$  stands for the activity coefficient of A. If the self-diffusivities and the dependence of  $\gamma$  on  $x$  are known for both A and B, we can then calculate the interdiffusivity as a function of  $x$ . This is exactly the idea of the self-diffusivity approach.

#### 2.4.2 Si and Ge self-diffusivity data

Si and Ge self-diffusivity ( $D_{Si}^*$  and  $D_{Ge}^*$ ) studies based on Si and Ge isotope diffusion have been reported since 1970's [88]. Especially, self-diffusivity of Ge in  $Si_{1-x}Ge_x$  alloys has been widely studied with different Ge isotopes [89-93]. Due to the shorter lifetimes of Si isotopes, however, there was little systematic study of Si self-diffusivity in  $Si_{1-x}Ge_x$  alloys until the studies by Kube *et al.* [92, 93]. In their work,  $D_{Si}^*$  and  $D_{Ge}^*$  were measured at six  $x_{Ge}$  values.

These data enabled the practice to establish a quantitative relation between  $D_{Si}^*$ ,  $D_{Ge}^*$  and  $\tilde{D}$ . However, these work only measured  $D_{Si}^*$  and  $D_{Ge}^*$  at six discrete  $x_{Ge}$  values. Some data interpolation was needed. An Arrhenius relation in Equation (8) was used, where  $D_{Si,0}^*$  and  $D_{Ge,0}^*$  are the prefactors and  $E_a$  is the activation energy. These three parameters are all  $x_{Ge}$  dependent.

$$D_j^*(x_{Ge}) = D_{j,0}^*(x_{Ge}) e^{\frac{-E_a(x_{Ge})}{kT}}, \quad j = Si \text{ or } Ge \quad (8)$$

To obtain practical  $D_{Si,0}^*$  and  $D_{Ge,0}^*$  in the full Ge range, we need to interpolate Kube *et al.*'s data.  $D_{Si,0}^*$  and  $D_{Ge,0}^*$  can be expressed as,  $D_{Si,0}^*(x_{Ge}) = \exp(a_0 + a_1 x_{Ge} - a_2 x_{Ge}^2)$  and  $D_{Ge,0}^*(x_{Ge}) = \exp(b_0 + b_1 x_{Ge} - b_2 x_{Ge}^2)$ , where  $a_0 = 6.489$ ,  $a_1 = 4.964$ ,  $a_2 = 7.829$ ;  $b_0 = 6.636$ ,  $b_1 = 8.028$ ,  $b_2 = 11.318$ . All these fitting parameters are dimensionless.

The activation energy  $E_a$  of self-diffusivity follows a modified Vegard's law shown in Equation (9), which is a second order dependence on  $x_{Ge}$  [93]. The parameters  $Q(0)$ ,  $Q(1)$  and  $\theta$  are all from



Ref. [93]. For Si self-diffusivity,  $Q(0)$ ,  $Q(1)$  and  $\theta$  are 4.76, 3.32 and 1.54 eV respectively. For Ge self-diffusivity, they are 3.83, 3.13 and 1.63 eV respectively.

$$Q_j(x_{Ge}) = (1-x_{Ge})Q_j(0) + x_{Ge}Q_j(1) + x_{Ge}(1-x_{Ge})\Theta_j, \quad j = Si \text{ or } Ge \quad (9)$$

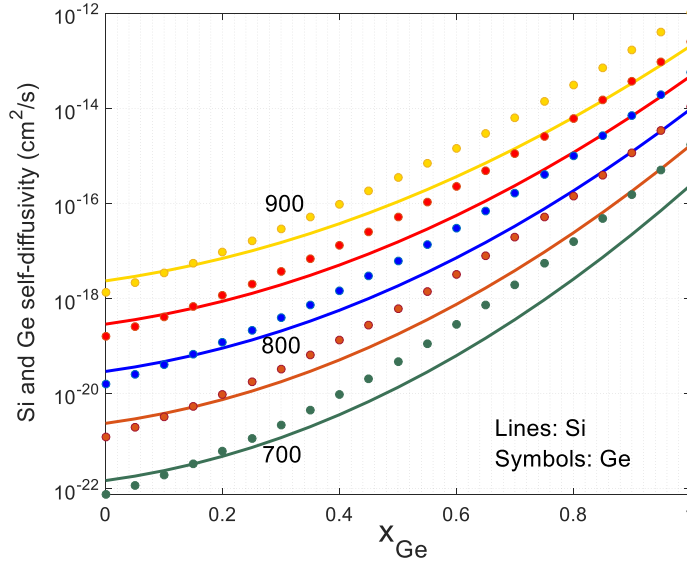


Figure 7. Calculated Si and Ge self-diffusivity values as a function of the Ge molar fraction in the temperature range from 700 to 900 °C based on Equation (8) and (9).

After  $D_{Si,0}^*$ ,  $D_{Ge,0}^*$  and  $E_a$  were modeled, we calculated the Si and Ge self-diffusivities using Equation (8) and (9). They show a good consistency with Kube *et al* and Strohm *et al*'s data. For the reader's convenience, Figure 7 plots the Si self-diffusivity and Ge self-diffusivity using the above parameters and models. It can be seen that there are 5 to 6 orders of magnitude difference between the self-diffusivities at the Si end and those at the Ge end.

### 2.4.3 Interdiffusivity calculations

SiGe solid solutions were assumed to be regular solutions, where the entropy of mixing is the same as that for an ideal solution. The partial molal enthalpy  $\overline{\Delta H}$  of Si and Ge in a SiGe solid solution is shown in Equation (10) [94], where  $\alpha$  is the interaction parameter. V. T. Bublik et al. measured  $\alpha$ , which is linear with  $x_{Ge}$  as in Equation (11) [95].  $\frac{\partial \ln \gamma}{\partial \ln x}$  for Si and Ge was calculated with Equation (12). Theoretically,  $\frac{\partial \ln \gamma}{\partial \ln x}$  should be identical for Si and Ge. The calculated results based on the experimental  $\alpha$  are quite close. The small difference between  $\frac{\partial \ln \gamma_{Si}}{\partial \ln x_{Si}}$  and  $\frac{\partial \ln \gamma_{Ge}}{\partial \ln x_{Ge}}$  is caused by the asymmetry of  $\alpha$  over Ge molar fraction. Finally,  $\tilde{D}_{Si-Ge}$  was calculated using Equation (7) and (12).

$$\begin{aligned} \overline{\Delta H}_{Si} &= R_g T \ln \gamma_{Si} = \alpha x_{Ge}^2 \\ \overline{\Delta H}_{Ge} &= R_g T \ln \gamma_{Ge} = \alpha (1-x_{Ge})^2 \end{aligned} \quad (10)$$

$$\alpha = 8787 - 1339x_{Ge} \text{ (J / mol)} \quad (11)$$

$$\frac{\partial \ln \gamma_{Si}}{\partial \ln x_{Si}} = \frac{(1 - x_{Ge})x_{Ge}(4017x_{Ge} - 17574)}{R_g T} \quad (12)$$

$$\frac{\partial \ln \gamma_{Ge}}{\partial \ln x_{Ge}} = \frac{(1 - x_{Ge})x_{Ge}(4017x_{Ge} - 18913)}{R_g T}$$

#### 2.4.4 The benchmarking interdiffusivity

As discussed above, Dong *et al.*'s model is based on Equation 7 to 12 shown above. This model applies to interdiffusion under no strain. 1% tensile strain was shown to have little impact on the interdiffusion for SiGe with up to  $x_{Ge} = 0.3$  [96]. The tensile strain impact can also be seen from Figure 6 (b). The extracted interdiffusivity in Figure 6 (b) are from different interdiffusion couples such as s-Si/r-Si<sub>0.8</sub>Ge<sub>0.2</sub>, s-Si/r-Si<sub>0.6</sub>Ge<sub>0.4</sub>, and s-Si/r-Si<sub>0.44</sub>Ge<sub>0.56</sub>. Here “s” means “strained”, and “r” means “relaxed”. The s-Si layers are under different tensile strains. If tensile strains have a significant impact, then the extracted interdiffusivity curves will not overlap or follow the same trend. Therefore, we conclude that tensile strain up to 1% has little impact.

The interdiffusivity at T = 900 °C calculated using Dong *et al.*'s model is shown in Figure 8, which agree with literature data and models very well. Dong *et al.*'s model also matches Gavelle *et al.*'s results well for  $x_{Ge} \geq 0.85$ . Samples in Gavelle *et al.*'s work have a high dislocation density ( $10^{10} \text{ cm}^{-2}$ ), while the samples in other literature work have dislocation densities in the  $10^5$  to  $10^6 \text{ cm}^{-2}$  range. Therefore, Si-Ge interdiffusion in Gavelle *et al.*'s work has a large dislocation-mediated interdiffusion component. This term dominates and results in a much faster interdiffusion in the low to medium  $x_{Ge}$  range. Besides the good agreement with literature data from multiple research groups, this model gave very good predictions for Si/Si<sub>1-x</sub>Ge<sub>x</sub> heterostructures under soak and spike rapid thermal annealing up to 1200 °C [70]. Its accuracy has been further confirmed with our later studies on strain and doping impacts as the benchmarking lines.

One thing to bear in mind is that Dong *et al.*'s model is based on the self-diffusivity data and their interpolation in Ref. [93]. The temperature range was from 880 to 1270 °C at  $x_{Ge} = 0$  end (the Si end), and 550 to 900 °C at  $x_{Ge} = 1$  end (the Ge end) correspondingly. Therefore, it is valid in this temperature range. We recommend to use Dong *et al.*'s model in 800 to 1300 °C range for low Ge alloys, in 700 to 1100 °C range for mid-Ge range alloys and in 500 to 900 °C for high-Ge alloys.

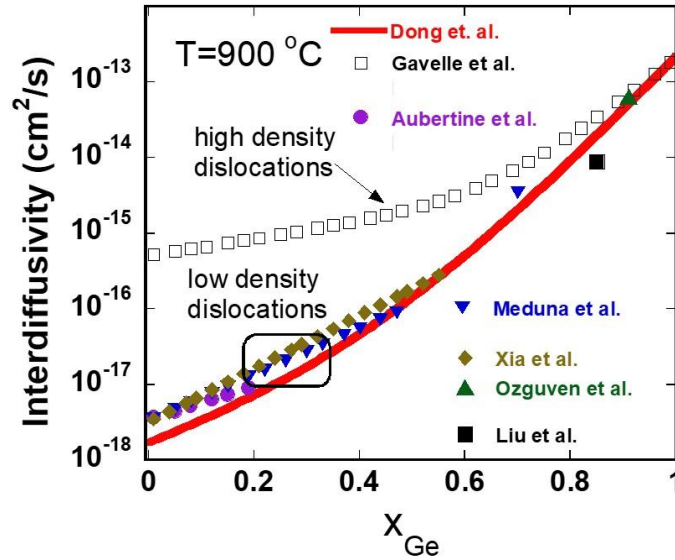


Figure 8. SiGe interdiffusivity at 900°C calculated using Dong *et al.*'s model in comparison with literature data and models. Figure adapted from Ref. [70] with from AIP Publishing. The literature data are from [71], [81-86].

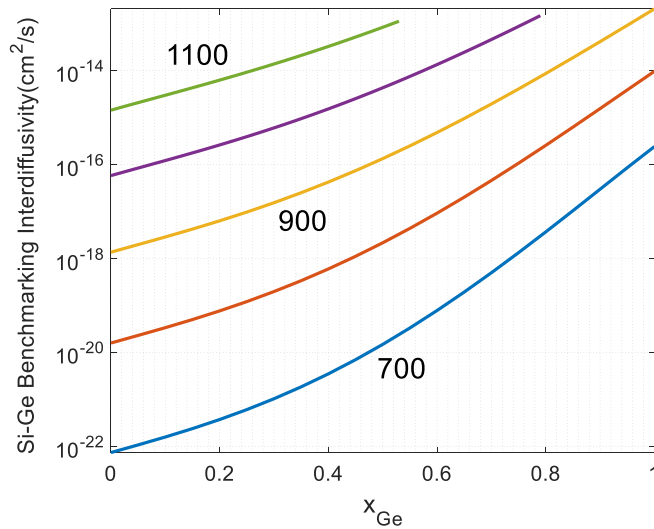


Figure 9. Calculated Si-Ge benchmarking interdiffusivity based on Dong *et al.*' model in [70] for 700 to 1100°C. These results apply to undoped, unstrained/tensile-strained SiGe systems with low defect densities (threading dislocation density  $< 10^7 \text{ cm}^{-2}$ ). They served as the benchmarking lines for later interdiffusion studies on strain and doping effects.

For the convenience of potential users, we provide more Si-Ge interdiffusivity curves in Figure 9, which has the interdiffusivity results calculated for the temperature range from 700 to 1100 °C with an interval of 100 °C. Readers can use Equation 7 to 12 to calculate the interdiffusivity of the temperatures of their interests.

As the melting temperature of Ge is 938.8 °C, above this temperature, the Ge molar fraction range for solid-state SiGe alloys doesn't extend to 100% Ge. For example, according to the solidus

line of the Si-Ge phase diagram under one atmosphere pressure, at 1000 °C,  $\text{Si}_{1-x}\text{Ge}_x$  alloys are solid when  $x < 0.79$ . At 1100 °C,  $\text{Si}_{1-x}\text{Ge}_x$  alloys are solid when  $x < 0.53$ . From Figure 9, we can see that the interdiffusivity  $\tilde{D}$  has a very strong dependence on  $x_{\text{Ge}}$ . From  $x_{\text{Ge}} = 0$  to 1, the interdiffusivity increases by 5 to 6 orders of magnitude in 700-900 °C for relaxed SiGe. The interdiffusivity  $\tilde{D}$  has a near-exponential relationship with  $x_{\text{Ge}}$  at the Si end and at the Ge end. The  $x_{\text{Ge}}$  dependence is stronger at the Ge end. Therefore, if the  $x_{\text{Ge}}$  range is limited as the case in [71]'s study, the interdiffusivity can be approximated as an exponential relation with  $x_{\text{Ge}}$ . In terms of the temperature dependence, 8-17X enhancement is observed for every 50 °C increase at the Si end, and 4-7X enhancement for every 50 °C at the Ge end in 700-900 °C as seen in Figure 10.

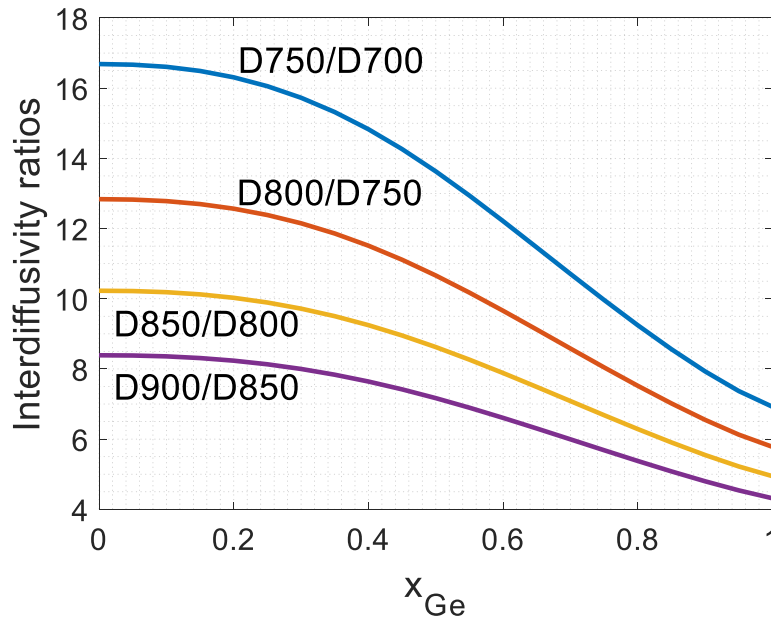


Figure 10. Interdiffusivity ratios showing the temperature dependence. The calculations are based on Dong et al.' model in [70].

### 3. Impacting Factors of Interdiffusion: Stress, Doping, Defect Engineering and Threading Dislocation Density

#### 3.1 Background and terms

In the above benchmarking Si-Ge interdiffusivity  $\tilde{D}$ , the temperature and Ge concentration are included. It is based on self-diffusivities, where tracer diffusion is measured in a chemically homogenous material with no strain, which is quite ideal. Stress, doping, defect engineering (such as oxidation and carbon incorporation) and defect density are all important impacting factors. These factors are very relevant to the industry practice. For example, in SiGe-channel p-type FinFETs shown in Figure 2, the SiGe channel is under compressive strain, and defects such as dislocations are unavoidable. In source and drain stressors for CMOS applications, SiGe stressors are normally highly doped. In SiGe HBTs, carbon and dopant coexist in compressive SiGe base layers. In Ge-on-Si lasers, the Ge layers are commonly tensile-stressed with high n-type doping and high defect density exists at the Ge/Si interfaces. Therefore, the studies on stress, doping, defect engineering and defect density are crucial to the industry practice.

Here, we need to clarify the term “defect engineering”. “Defect” is a generic term, which include defects of 0D, 1D, 2D and 3D forms. When using the term “defect engineering” in the context of diffusion in semiconductors, point defects are commonly referred, which can be engineered using oxidation, nitration and carbon incorporation to tweak the point-defect-mediated diffusion and thus dopant or alloy concentration distributions.

Dislocations are line defects, which add a dislocation-mediated term on top of the point-defect-mediated term. The modeling shown above in Equation 7 to 12 has no dislocation-mediated term, as it refers to SiGe material systems with low threading dislocation densities ( $< 10^{16} \text{ cm}^{-3}$ ). Threading dislocations are dislocations with a component vertical to the lattice-mismatch planes. For the experiments involved, due to the 1D nature of epitaxy growth direction and the profiling technique direction such as SIMS, diffusion in the out-of-plane direction is commonly designed and measured, which is 1D diffusion. For more practical 2D and 3D material systems such as SiGe source and drain regions, diffusion can be calculated using a finite element method and transport equations established and calibrated using 1D diffusion data.

#### 3.2 Summary of major findings

Table 1 summarizes major discoveries on the Si-Ge interdiffusion impacting factors for the readers.

Topics	Main discoveries
Undoped, low-defect and unstrained SiGe interdiffusivity	A unified Si-Ge interdiffusivity model for the full Ge range was built, and verified by data and literature work [70]. a) $\tilde{D}$ has a near-exponential relationship with $x_{Ge}$ at the Si and Ge ends with different slopes. From $x_{Ge} = 0$ to 1, the interdiffusivity

		increases by 5 to 6 orders of magnitude in 700-900 °C for relaxed SiGe. b) 8-17X enhancement is observed for every 50 °C increase at the $x_{Ge} = 0$ end, and 4-7X enhancement for every 50 °C at the $x_{Ge} = 1$ end in 700-900 °C.
Compressive strain impact		$\tilde{D}$ depends exponentially on compressive strain [71], [72].
Tensile strain impact		Not observable for structures with up to 30% Ge with 1% tensile strain [96].
Compressive strain relaxation effect		When the strain relaxation history is known, this effect can be modelled as a smaller strain in the compressive strain term [72].
Threading dislocation impact		It introduces a dislocation-mediated interdiffusion term, which is significant for low Ge regimes [72].
Doping and impurity impact		P, C and As enhances interdiffusion. B has a small impact. N-doping effect can be modelled as a Fermi effect [5, 58, 97].
Defect engineering by carbon		1.2% carbon enhances interdiffusion of Si/Si <sub>0.79</sub> Ge <sub>0.21</sub> superlattices [97].
Defect engineering by oxidation		Not observable for structures with Ge 15-60% with a -1% compressive strain [98]

**Table 1. Summary of the influences from impacting factors of Si-Ge interdiffusion.**

The interdiffusivity models and data generated in Xia et al. and Dong et al.'s work have been widely used and implemented in the state-of-the-art process simulation tools including Intel's in-house process simulation tool, Crosslight Software's CSUPREM™ and Synopsys's Sentaurus Process™ (the leading commercial 3D process simulation tool in the semiconductor industry), and Lumerical's DEVICE™ for structure and process design of next generations of semiconductor device.

### 3.3 Biaxial strain impacts

For SiGe systems, Si is commonly used as the substrate. Therefore, SiGe layers are commonly under compressive strains. For MOSFET applications, tensile strains are desired for n-type MOSFETs for electron mobility enhancement and compressive strain are desired for hole mobility enhancement. External stress liners and/or source and drain stressors can be used to introduce strains in the channels.

Xia et al.'s work in 2006 studied the stress impact on the interdiffusion, and observed that tensile stress has little impact, where compressive stress enhances interdiffusion significantly [96]. There have been little studies on the tensile strain impact on interdiffusion other than [96], which shows that up to 1% biaxial tensile strain has little impact on the interdiffusion where compressive biaxial strains increase interdiffusion significantly (Figure 11).

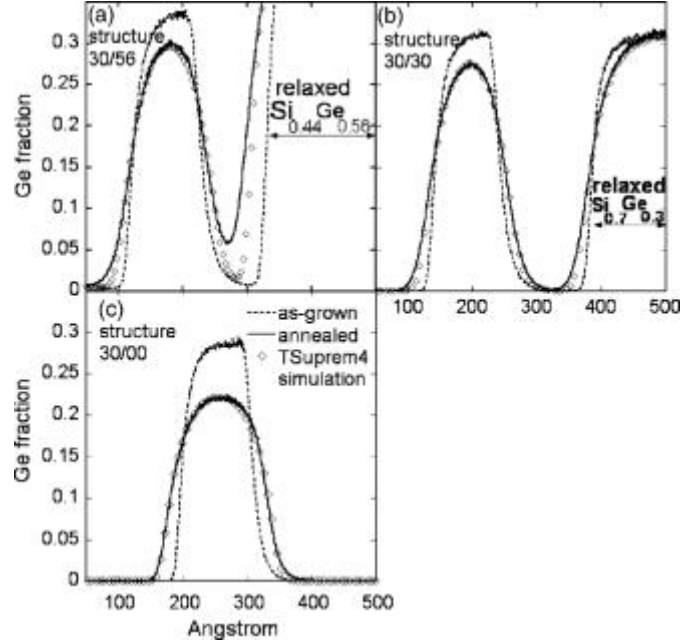


**Figure 11.** As-grown and annealed SIMS profiles of  $\text{Si}_{0.70}\text{Ge}_{0.30}$  peaks on (a) relaxed  $\text{Si}_{0.44}\text{Ge}_{0.56}$ , (b) relaxed  $\text{Si}_{0.70}\text{Ge}_{0.30}$ , and (c) Si substrates. The annealing condition is  $880^\circ\text{C}$  for 90 min. Comparison of the profiles in (a) and (b) indicates that tensile strain in the  $\text{Si}_{0.70}\text{Ge}_{0.30}$  has little impact on interdiffusion, while compressive strain is associated with a large interdiffusion enhancement [comparison of profiles in (b) and (c)]. Figure reproduced from [96] with permission from AIP publishing.

The stress/strain impact on Si-Ge interdiffusion is an interesting topic. Is the stress gradient an extra driving force for interdiffusion on top of the chemical gradient driving force? Does the stress impact the activation energy and the pre-factor of interdiffusivity? Is the impact from stress gradient or from the stress-related defects? Quantitatively, what is the magnitude of the impact? How can it be modeled? These topics were systematically investigated in [72]. The  $x_{\text{Ge}}$  studied ranged from 0.36 to 0.75, and the temperature range was  $720\text{--}880^\circ\text{C}$ . The form of strain is biaxial strain, which is naturally formed in epitaxial SiGe structures. In the industry practice, although stress/strain can be 3D distributions. In a lot of cases, the stress/strain distributions can be approximated as biaxial strain distributions. The epitaxial SiGe structures were kept pseudomorphic during the annealing.

### 3.3.1 Biaxial strain impact on the driving force of interdiffusion

Theoretical analysis in [72] showed that a biaxial strain field adds a term to the interdiffusion driving force on top of the driving force from the chemical concentration gradient. With some derivations using the Gibbs free energy contributions from chemical mixing, elastic biaxial strain, chemical gradient energy and elastic gradient energy, this effect can be included in an apparent interdiffusivity  $\tilde{D}_{\text{apparent}}$  as defined below in (13).

$$\tilde{D}_{\text{apparent}} = \tilde{D}^{\text{strained}} \left( 1 + \frac{2V_m \eta^2 Y_{UVW}}{G_c''} \right) \quad (13)$$

In the above equation,  $\tilde{D}^{strained}$  is the interdiffusivity under a biaxial strain.  $V_m$  is the molar volume of the solid solution, and for SiGe,  $V_m \approx 13 \text{ cm}^3/\text{mol}$ .  $\eta$  is the lattice mismatch. It is 0.0418 for Si and Ge.  $Y_{UVW}$  is the biaxial modulus, which equals  $E/(1 - \nu)$ .  $E$  is Young's modulus, and  $\nu$  is the Poisson ratio.  $G_c''$  is the second derivative of the Gibbs free energy term for chemical mixing over  $x_{Ge}$ . The term  $\frac{2V_m\eta^2Y_{UVW}}{G_c''}$  reflects the magnitude of the biaxial strain energy contribution to the driving force, which depends on  $x_{Ge}$  and temperature. Figure 12 has the strain field effect term  $\frac{2V_m\eta^2Y_{UVW}}{G_c''}$  as a function of  $x_{Ge}$  and temperature. For  $x_{Ge} = 0.5$  at 1000 K, for example, this term can be as large as 0.33, so the strain contribution to the driving force should not be neglected [98, 99]. When  $x_{Ge}$  is close to 0 or 1 at high temperatures, this factor is negligible.

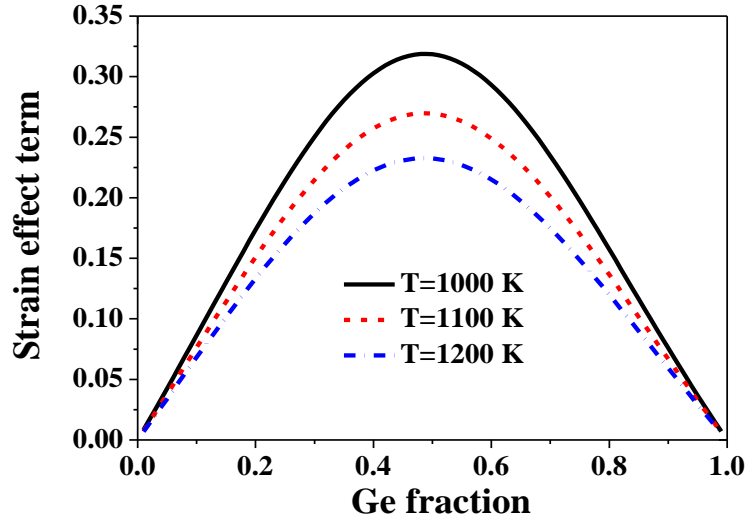


Figure 12. Ge concentration dependence of the strain effect term  $\frac{2\eta^2Y_{UVW}}{f_0''}$  at different temperatures.

For epitaxial SiGe systems with  $\langle UVW \rangle = \langle 100 \rangle$ , it can be shown that:

$$\tilde{D}_{apparent} = \left(1 + \frac{2 \times 0.0418^2 Y_{100}}{f_0''}\right) \tilde{D}^{strained}. \quad (14)$$

In the above equation,  $Y_{100}$  is the biaxial modulus of (100) orientation Si<sub>1-x</sub>Ge<sub>x</sub>;  $f_0(x_{Ge})$  is the Helmholtz free energy per unit volume of the homogeneous solution, and  $\tilde{D}^{relax}$  is the interdiffusivity with no strain. The calculation of  $f_0''$  can be found in [72].

### 3.3.2 Biaxial strain impact on the interdiffusivity

Besides the change in the driving force, strain can change  $\tilde{D}^{strained}$  itself. The definition of the strain derivative of the interdiffusivity,  $q'$ , is shown in Equation (15). It includes the effects of strain on the diffusivity prefactors and on the activation energy.



$$q'(T) \equiv - \left( \frac{kT}{\varepsilon} \right) \ln \left( \frac{\tilde{D}^{strained}}{\tilde{D}^{relax}} \right) \quad (15), \text{ and thus}$$

$$\tilde{D}^{strained} = \tilde{D}^{relax} e^{\frac{-q'\varepsilon}{kT}} \quad (16)$$

Taken the strain relaxation factor R into account, the apparent interdiffusivity can be expressed as:

$$\tilde{D}_{apparent} = \left( 1 + \frac{2\eta^2(1-R)^2 Y_{UVW}}{f_0''} \right) \tilde{D}^{relax} e^{\frac{-q'\varepsilon_0(1-R)}{kT}} \quad (17)$$

$\varepsilon_0$  is the strain without any relaxation.  $q'$  was quantitatively extracted from the experimental data in [72] as:

$$q' = (-0.081T + 110)\text{eV}. \quad (18)$$

Therefore, the interdiffusivity under a biaxial compressive strain can be expressed as:

$$\tilde{D}^{strained} = \tilde{D}^{relax} e^{\frac{-q'\varepsilon}{kT}} = \tilde{D}^{relax} e^{\frac{(0.081T-110)\text{eV}\varepsilon}{kT}} \quad (19)$$

Table 2 summarizes all the  $q'$  value from literature. Dong *et al.*'s work extended the Ge fraction range to 0.75, and  $q'$  value from that work is comparable to other  $q'$  values reported at lower Ge fraction ranges. There are little systematic data on the  $x_{Ge}$  dependence of  $q'$ . Overall,  $q'$  is in the range of 10 to 45 eV/unit strain. More experimental studies for different Ge fractions and temperatures are needed.

References	$x_{Ge}$	Maximum compressive strain $\varepsilon$	Temperature (°C)	$q'$ (eV/unit strain)
Cowern <i>et al.</i> [74]	0.25	-1.05%	900 — 1050	35 — 45
Cowern <i>et al.</i> [100]	0.3	-1.26%	875	13.5 — 22.1
Aubertine <i>et al.</i> [101]	0.17	-0.71%	795 — 895	19
Aubertine <i>et al.</i> [81]	0.075 — 0.19	-0.81%	770 — 870	10
Xia <i>et al.</i> [71]	0.30 — 0.56	-1.05%	770 — 920	27.6 — 36.3
Dong <i>et al.</i> [72]	0.36 — 0.75	-1.20%	720 — 880	16.6 — 29.6

**Table 2. Experimental values of the strain derivative of the interdiffusivity  $q'$  in Si-Ge interdiffusion.**

$q'$  includes the impact of strain on both Ge and Si diffusion. For Dong et al's samples with medium Ge fraction, not only  $x_{Ge}$  and  $1-x_{Ge}$ , but also Ge and Si self-diffusivities are comparable, so the impact of strain on Ge diffusion and Si diffusion both contribute to  $q'$ . As is known, on the atomic scale, Si and Ge diffusion in SiGe can be mediated by either interstitials or vacancies, or both. Theiss et al. and Aziz et al. has shown that compressive strain enhances vacancy mediated diffusion while retards interstitial mediated diffusion [102, 103]. Therefore,  $q'$  for Si-Ge interdiffusion should also depend on the I- and V-mediated fractions, which depend on both temperature and Ge fraction. In Si and Si rich SiGe, Si and Ge self-diffusion are mediated by both interstitials and vacancies [48, 88, 90, 104].

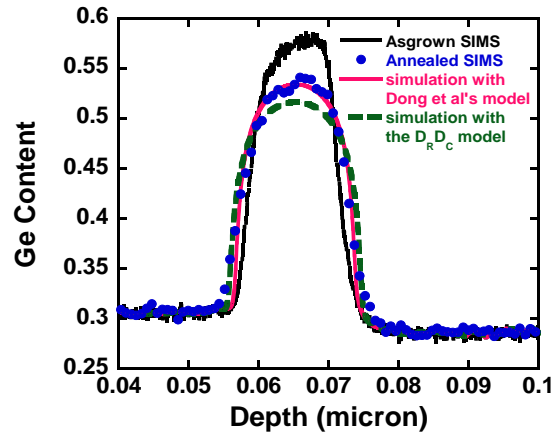


Figure 12 (a) As-grown, annealed Ge SIMS profiles of a  $Si_{0.70}Ge_{0.30}/Si_{0.45}Ge_{0.55}/Si_{0.70}Ge_{0.30}$  heterostructure and predictions simulated by Dong's model [70] and  $D_R D_C$  [71]. The furnace annealing was performed at 800 °C for 40 minutes. Figure reproduced from [105] with permission from Taylor and Francis Group.

Compared with the  $D_R D_C$  model in Equation (4) and (5) [71], which is a good empirical model, the compressive strain impact in Dong *et al*'s 2014 work [70] is more scientifically sound in terms of thermodynamics and diffusion theory, and should work for a larger temperature range. In terms of practical application, both models give reasonable predictions within the error bar. Predictions from both models are compared with SIMS data, shown in Figure 12.

### 3.4 Doping impacts

For HBT applications, the Ge molar fraction is commonly below 0.3, and SiGe layers are typically tens of nanometer thick and under compressive strain. P and B were shown to enhance Si-Ge interdiffusion in Si/Si<sub>0.8</sub>Ge<sub>0.2</sub> (Figure 13) [97]. Carbon is not a dopant, but it also increases the interdiffusion as seen in Figure 13 (d).

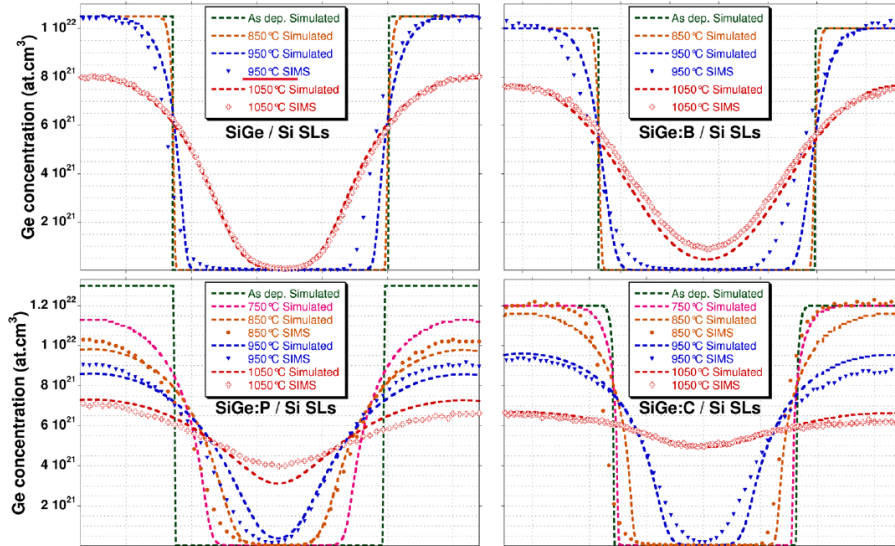


Figure 13. TOF-SIMS as-deposited and annealed Ge profiles of the first valley of SiGe/Si, SiGe:B/Si, SiGe:P/Si and SiGe:C/Si superlattices. Figure reprinted from [97] with permission from AIP publishing.

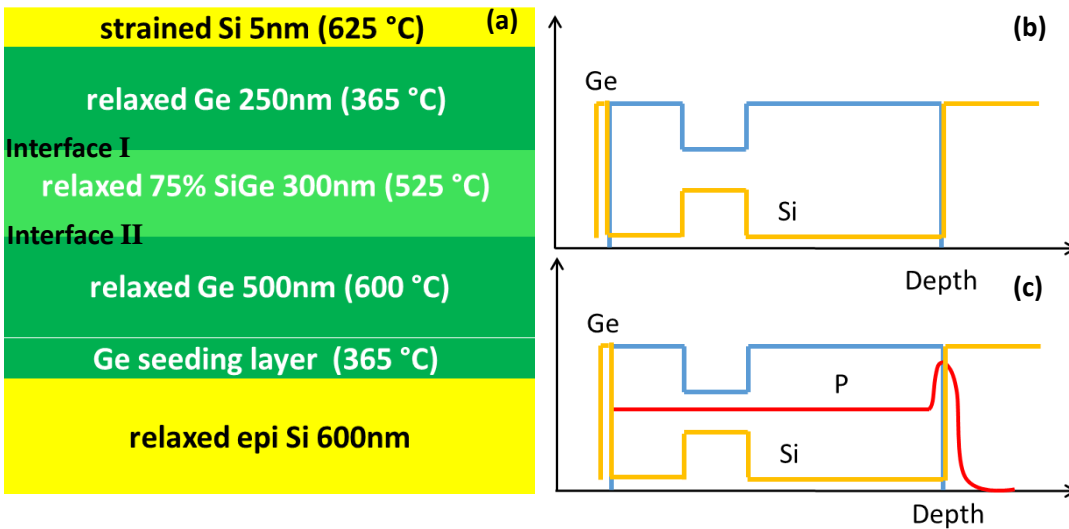


Figure 14. Samples used for the doping effect study: (a) sample structure and growth temperature (b) depth profile of the sample with no P doping and (c) depth profile of the sample with P doping concentration at around  $5 \times 10^{18} \text{ cm}^{-3}$ . Figure reprinted from [58] with permission from AIP publishing.

For Ge-on-Si laser applications, Ge is close to 100% Ge. The thickness is commonly a few hundred of nanometers resulting in fully relaxed Ge films on Si. A high n-type doping is typical and the interdiffusion has a significant impact on the light emission processes. In terms of the chemical composition, Ge-on-Si forms an interdiffusion couple that is a convenient structure for interdiffusion study. However, common epitaxial Ge/Si interfaces are highly defected due to the Ge seeding layers that are grown to reduce the dislocation density of the top Ge layers. Dopant

diffusion, dopant segregation and interdiffusion are coupled and hard to separate or measure by SIMS. Therefore, Ge-on-Si structures are not ideal for interdiffusion studies.

To address this problem, Ref. [58] investigated the P doping effect on interdiffusion with Ge/Si<sub>1-x</sub>Ge<sub>x</sub>/Ge on Si structures (Figure 14) such that the highly-defected Ge/Si interfaces are sufficiently away from the interdiffusion region of our interest. The samples have 0.75 < x<sub>Ge</sub> < 1 and a mid-10<sup>18</sup> to low-10<sup>19</sup> cm<sup>-3</sup> P doping. The dislocation densities were around 10<sup>8</sup> to 10<sup>9</sup> cm<sup>-2</sup> range. The P-doped sample shows an accelerated Si-Ge interdiffusivity, which is 2-8 times of that in the undoped sample. As Interface I and II, the interdiffusion regions of our interests, are not at the Ge/Si interfaces, the dislocation density in this study was assume to be not significant, and the dislocation mediated diffusion was ignored for this case. The doping dependence of the Si-Ge interdiffusion was modelled by a Fermi-enhancement factor “FF”.

$$\tilde{D}_{total} \approx \tilde{D}_{lattice,undoped} * FF = \tilde{D}(n = n_i) * FF \quad (19)$$

$$FF \equiv \frac{\tilde{D}(n)}{\tilde{D}(n_i)} = \frac{1+m_1 \exp\left(\frac{E_i-E_{V^-}}{kT}\right)\left(\frac{n}{n_i}\right)+m_2 \exp\left(\frac{2E_i-E_{V^-}-E_{V^{2-}}}{kT}\right)\left(\frac{n}{n_i}\right)^2}{1+m_1 \exp\left(\frac{E_i-E_{V^-}}{kT}\right)+m_2 \exp\left(\frac{2E_i-E_{V^-}-E_{V^{2-}}}{kT}\right)} \quad (20)$$

Here, we denote:

$$\beta = m_1 \exp\left(\frac{E_i-E_{V^-}}{kT}\right), \quad (21)$$

$$\gamma = m_2 \exp\left(\frac{2E_i-E_{V^-}-E_{V^{2-}}}{kT}\right), \quad (22)$$

$E_i$ ,  $E_{V^-}$ , and  $E_{V^{2-}}$  are the electron energy levels for intrinsic SiGe, single negatively charge vacancies and double negatively charged vacancies. The experiments show that Si-Ge interdiffusion coefficient is proportional to  $n^2/n_i^2$  for 0.75 < x<sub>Ge</sub> < 1. This indicates that the interdiffusion in high Ge fraction range with n-type doping is dominated by V<sup>2-</sup> defects. FF was shown to have a relatively weak dependence on the temperature and x<sub>Ge</sub>.  $m_1 = 1$  and  $m_2 \geq 20$  generate good fitting to the experimental data (Figure 15).

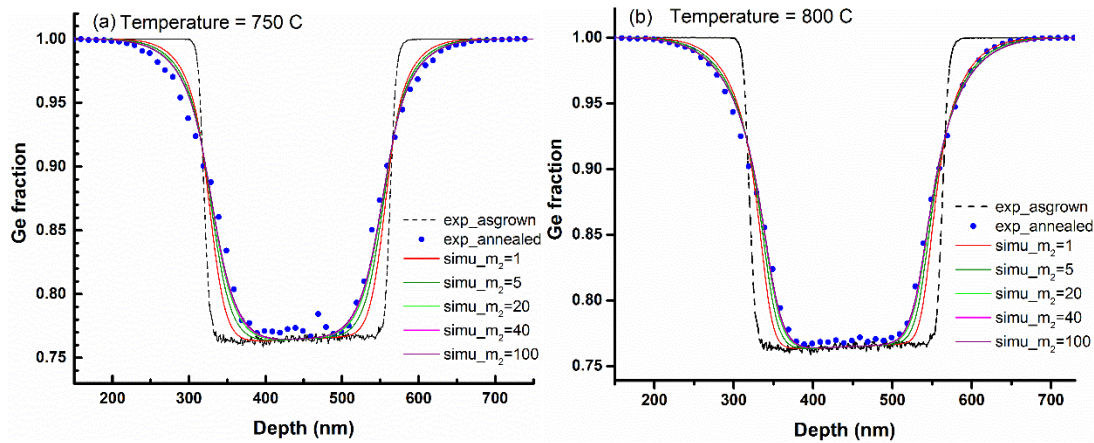


Figure 15 Comparison between SIMS data and calculations using Equation (19) to (22). Ge profile fitting (a) at 750 °C for 120 minutes; (b) at 800 °C for 30 minutes.  $m_1$  is fixed to 1 in each simulation and  $m_2$  is 1, 5, 20, 40, 100 separately. Figure reprinted from [58] with permission from AIP publishing.

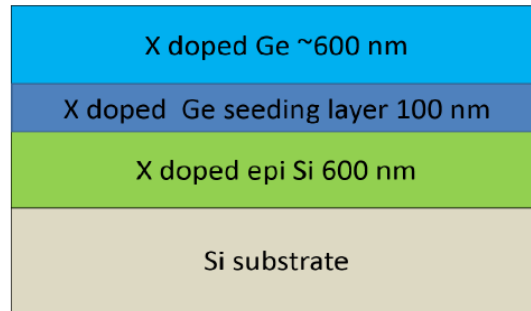


Figure 16 Epitaxial structure used in [73] to study the doping impact on material quality and Si-Ge interdiffusion. X stands for As, higher boron, lower boron, phosphorus-doped or undoped. Figure reprinted from [73], an open access paper by OSA Publishing.

[73] further investigated Ge-on-Si epitaxial film quality and interdiffusion with three different dopants (P, As and B) and those without intentional doping for the full Ge range. Some have seen a high temperature (nominal 850 °C) and low temperature (nominal 680 °C) thermal cycling defect annealing step, while some have not. The doping levels after defect annealing can be found in Figure 16 (b). All samples have a smooth surface (roughness < 1.5 nm), and the Ge films are almost entirely relaxed. Etch pit density (EPD) data have been obtained for the doped Ge, which shows that boron-doped Ge has the highest EPD in  $10^8 \text{ cm}^{-2}$ .

Caution needs to be taken when using EPD as a TDD characterization method [106]. Although EPD methods have been used to give rough estimations of TDD in undoped Ge, it can generate large discrepancies for doped Ge due to the change in the etching property, where a significant portion of TDD do not show as etch pits. In these cases, electron channeling contrast imaging (ECCI) can be used, which is a SEM-based non-destructive characterization technique. In ECCI, the intensity of electrons backscattered from the surface of the sample under investigation is imaged [107]. Slight deformations of the crystal lattice, such as the strain field associated with dislocations, lead to a strong modulation of the backscatter intensity which can be observed using a backscatter detector. Differences between EPD and ECCI results can be orders of magnitude. For example, for P-doped Ge without defect annealing, EPD measured was  $3 \times 10^5 \text{ cm}^{-2}$ , while ECCI measured TDD was  $5.2 \times 10^8 \text{ cm}^{-2}$ . These TDD are measured from the top surface of Ge, which is a good indication of Ge film quality.

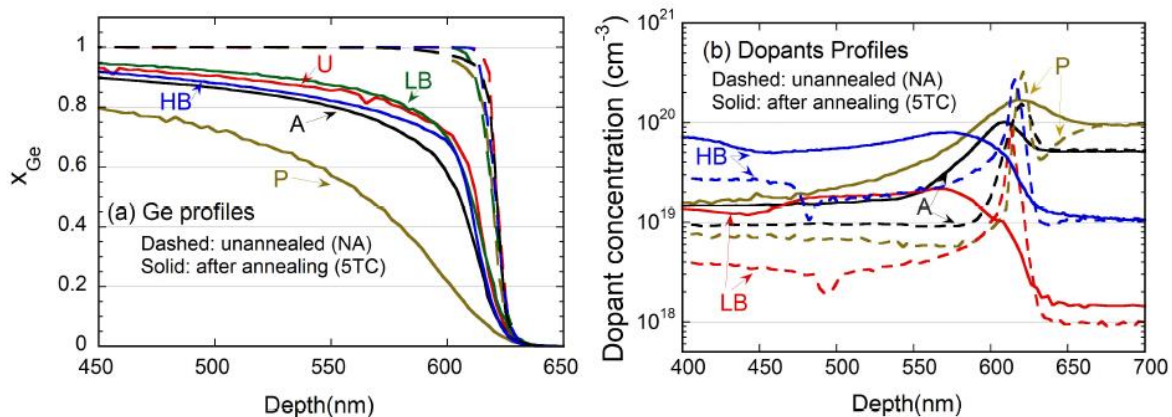


Figure 17. Ge and dopant profiles measured by SIMS showing the impact from different doping. A, HB, LB, P and U stand for As, higher boron, lower boron, phosphorus-doped or undoped Ge/Si sample. Figure reprinted from [73], an open access paper by OSA Publishing.

Before annealing, all samples have very similar sharp Ge profiles (Figure 17) and dopants have the highest concentration peaks at the interface of Ge/Si. This is due to the segregation induced by a high density of defects in the Ge seeding layers. Extracted effective interdiffusivity with different doping are shown in Figure 18. Sample P has the most interdiffusion. Sample A has the second largest interdiffusion. Sample U and sample LB have the least interdiffusion. For sample HB, it has no significant difference over sample LB in  $x_{Ge} < 0.7$  part, but it distinguishes itself from LB and U in  $x_{Ge} > 0.7$  part. The interdiffusion profiles are more box-like than Gaussian profiles, showing a strong dependence.

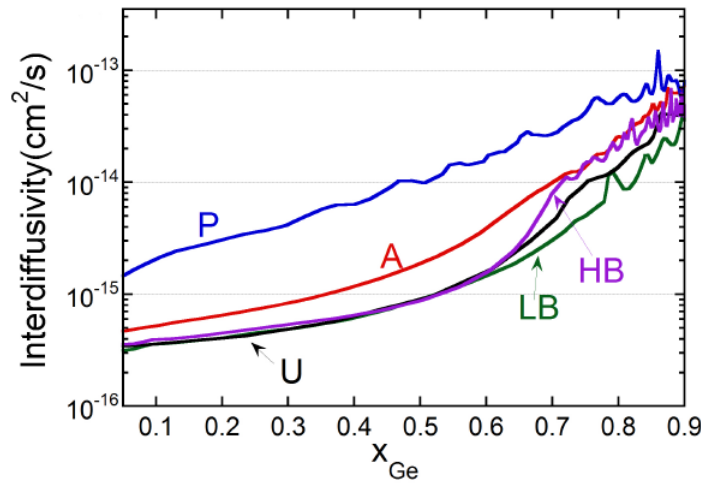


Figure 18. Extracted effective interdiffusivity with different doping. A, HB, LB, P and U stand for As, higher boron, lower boron, phosphorus-doped or undoped Ge/Si sample. Figure reprinted from [73], an open access paper by OSA Publishing.

In the interdiffusion region of the interest, which is at Ge seeding layer/Si interfaces, dislocation density is much higher due to the high lattice mismatch. Therefore, unlike the study in [2016 Cai], the dislocation mediated term can't be ignored in the modeling. Therefore, the total interdiffusivity is expressed as the following.

$$\tilde{D}_{total} = \tilde{D}_{dislocation} + \tilde{D}_{lattice,undoped} * FF \quad (23)$$



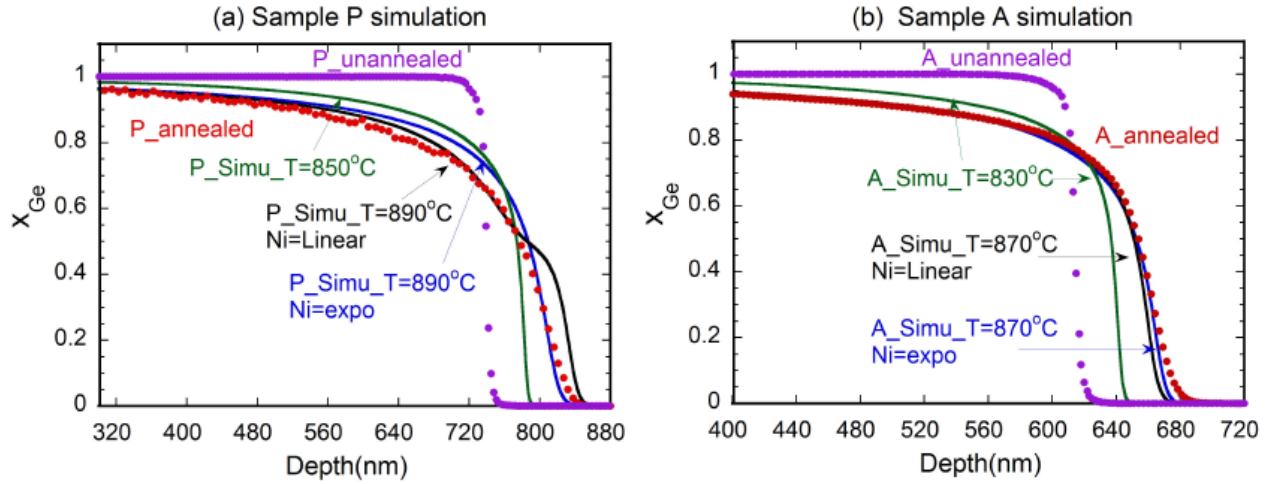


Figure 19. Fitting of Ge profiles with different  $n_i$  modeling and/or temperatures. (a) P-doped Ge and (b) As-doped Ge. Figure reprinted from [73], an open access paper by OSA Publishing.

Due to limited data of  $n_i(x_{Ge})$ , Cai et al. used linear interpolation between  $n_{i,Ge}$  and  $n_{i,Si}$  as in Equation (24), which is good enough for  $0.75 < x_{Ge} < 1$ .

$$n_i(x_{Ge}) = n_{i,Ge}x_{Ge} + n_{i,Si}(1 - x_{Ge}) \quad (24)$$

However, Zhou et al.'s work covers  $0 < x_{Ge} < 1$  range. According to [108], Zhou et al. compared the linear and the exponential interpolation between  $n_{i,Ge}$  and  $n_{i,Si}$  as shown in Equation (25).

$$n_i(x_{Ge}) = n_{i,Si} \exp\left(\ln \frac{n_{i,Ge}}{n_{i,Si}} \times x_{Ge}\right) \quad (25)$$

As illustrated in Figure 19, the exponential relation between the intrinsic carrier concentration  $n_i$  and  $x_{Ge}$  gives better Ge profile fitting results for P-doped and As-doped Ge/Si.

On the light emitting properties of doped Ge, photoluminescence (PL) measurements show that P and As doped Ge without defect annealing show a 5 to 10 times enhancement in PL intensity owing to the fact that the interdiffusion is minimized for unannealed samples, which have higher TDD but less Si-Ge intermixing [5].

### 3.5 Defect impacts

Thermal oxidation of silicon and carbon incorporation are both considered as one of the major approaches in changing point defect concentrations. The former one is to inject interstitials and the latter one is to consume interstitials and increase vacancy concentrations. The oxidation impact on interdiffusion was investigated by Ozguven et al. and by Xia et al. [71, 109]. The former one studied  $\text{Si}_{0.89}\text{Ge}_{0.11}$  and  $\text{Si}_{0.94}\text{Ge}_{0.06}$  superlattices coherent to a Si substrate, which showed a 123% enhancement in the interdiffusivity at 795 °C. The latter one studied compressively strained  $\text{Si}_{0.41}\text{Ge}_{0.59}$  and  $\text{Si}_{0.56}\text{Ge}_{0.44}$  layers with about -1% compressive strain. Interdiffusion under an effective inert, i.e., underneath masking layers, and oxidizing conditions showed no differences (Figure 20).

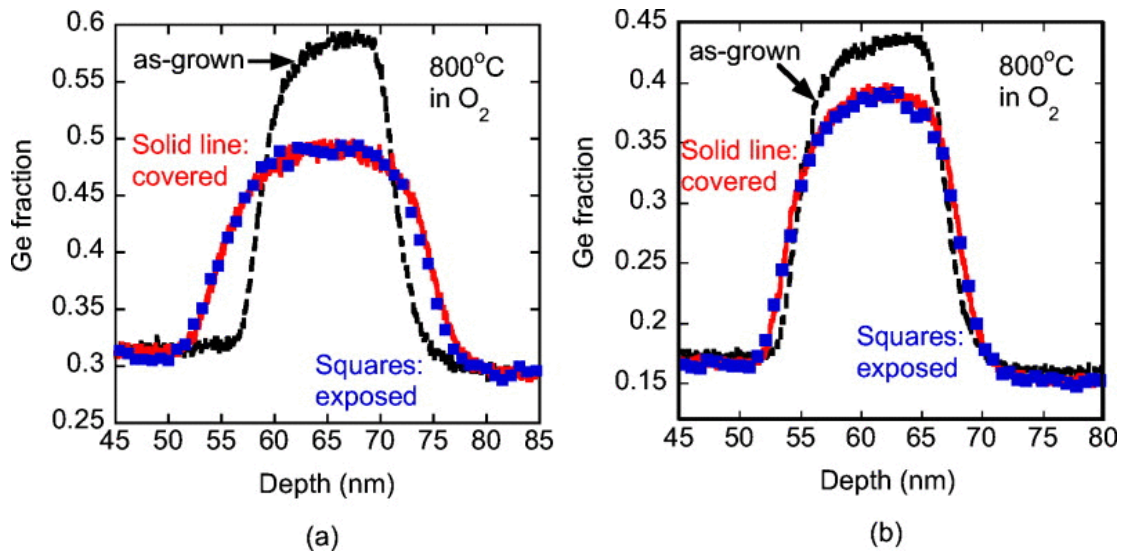


Figure 20. Ge SIMS profiles of (a) sample 30/59/30 and (b) sample 15/44/15, both are on a Si substrates. The annealing was performed at 800 °C for 40 min in oxygen. The solid line shows the profile covered by masking layers, and the squares indicate the profile measured under oxidizing conditions. Figure reprinted from [98] with permission from AIP publishing.

The effect of carbon is shown Figure 13 (d) above. The carbon used has a total concentration of  $6 \times 10^{20} \text{ cm}^{-3}$ , and the substitutional carbon was about  $4.6 \times 10^{20} \text{ cm}^{-3}$ . The total carbon level is 1.2 at.%, which is much larger than the common carbon level of less than 0.3 at.% used in SiGe HBTs. Nevertheless, this carbon impact supports a vacancy-mediated interdiffusion mechanism.

Besides the point defects, dislocations are common 1D defects in epitaxial SiGe systems. They serve as fast interdiffusion paths, which add a dislocation-mediated interdiffusion term as discussed previously.

#### 4 Summary and prospective

Over the past years, significant efforts have been devoted to answer this seemingly basic and fundamental question: for Si and Ge, the two very important and closely related semiconductors, how do they intermix. Getting the answers has taken many years when we tried to answer it in the atomic scale. So far, Si-Ge interdiffusion has been studied from a general point of view, where large ranges of impacting factors were studied. More detailed studies can be done for specific applications in the future. A constraint of interdiffusion studies lies in the constraint of the 1D profiling technique, its accuracy and planar diffusion structures. Many industry structures have 3D strain fields and 3D element distributions, but we have not been able to study those structures experimentally due to the constraint, although 3D predications can be done with the interdiffusion models and parameters calibrated with 1D structures. Atom probe tomography (APT) can obtain 3D element distributions. However, the cost is very high. Interdiffusion in Ge-Sn



systems is much less studied, which are also topics for the future work. After that, can we find a way to slow down the interdiffusion?

## **5 Conflict of interest**

The author declares that they have no conflict of interest.

## **6 Acknowledgements**

The author would like to acknowledge Natural Science and Engineering Research Council of Canada (NSERC), Crosslight Software Inc. and Lumerical Solutions for funding the Si-Ge interdiffusion studies at UBC. Crosslight Software Inc. and Lumerical Solutions are acknowledged for their technical assistance in implementing the interdiffusion models in their simulation tools CSUPREM™ and DEVICE™. The epitaxial structures of these studies were grown by Gary Riggott at the Microsystems Technology Laboratories at MIT, and Dr. Kwang Hong Lee in Prof. Chuan Seng Tan's group at Nanyang Technological University in Singapore. The Nanofabrication facility at UBC, Mattson Technology Canada and the Semiconductor Defect Spectroscopy Laboratory at Simon Fraser University are acknowledged for the technical assistance in the material processing and characterizations. CMC Microsystems is acknowledged for their support in Synopsys's Sentaurus Process and TSUPREM-4 usage. Dr. Stephen P. Smith at Evans Analytical Group is acknowledged for helpful discussions on SIMS analysis. Tao Fang in the Department of Materials Engineering at UBC is acknowledged for his help in proof-reading this paper.

## References

1. World Semiconductor Trade Statistics report 2017
2. Xia GR, et al. Impact of ion implantation damage and thermal budget on mobility enhancement in strained-Si n-channel MOSFETs. *IEEE Transactions on Electron Devices*, 2004. 51(12): p. 2136-2144.
3. Jung JW, et al. Effect of thermal processing on mobility in strained Si/strained Si<sub>1-y</sub>Ge<sub>y</sub> on relaxed Si<sub>1-x</sub>Ge<sub>x</sub> (x < y) virtual substrates. *Applied Physics Letters*, 2004. 84(17): p. 3319-3321.
4. Dehlinger G, et al. High-speed germanium-on-SOI lateral PIN photodiodes. *IEEE Photonics Technology Letters*, 2004. 16(11): p. 2547-2549.
5. Zhou G, et al. Improved Thin Film Quality and Photoluminescence of N-Doped Epitaxial Germanium-on-Silicon using MOCVD, unpublished data, 2018.
6. Liu J, et al. Tensile-strained n-type Ge as a gain medium for monolithic laser integration on Si. *2007 Opt. Exp.* vol. 15 no. 18 pp. 11272-11277.
7. Nam D, Strained Germanium Technology for On-chip Optical Interconnects. Doctoral dissertation, Stanford University, America, 2013.
8. Zaima S, Nakatsuka O, Taoka N, Kurosawa M, Takeuchi W and Sakashita M, "Growth and applications of GeSn-related group-IV semiconductor materials". *Science and Technology of Advanced Materials Sci Technol Adv Mater*, 16 (2015), p. 043502
9. Rücker H, et al. Suppressed diffusion of boron and carbon in carbon-rich silicon. *Appl. Phys. Lett.*, 1998, vol. 73, pp. 1682–1684.
10. Scholz R, Gösele U, Huh JY, and Tan TY, Carbon-induced undersaturation of silicon self-interstitials, *Applied Physics Letters*, 1998 vol. 72, pp. 200–202.
11. Rücker H, et al. Dopant diffusion in C-doped Si and SiGe: physical model and experimental verification. *IEEE Int. Electron Devices Meeting Technical Digest*, 1999, pp. 345 –348.
12. Bedell SW, et al. New opportunities for SiGe and Ge channel p-FETs. *Microelectronic Engineering*, 2011. 88(4): p. 324-330.
13. Wu YH, and Chin A, High temperature formed SiGe p-MOSFETs with good device characteristics. *Electron Device Letters, IEEE*, 2000. 21(7): p. 350-352.
14. Chern W, et al. High mobility high-k-all-around asymmetrically-strained Germanium nanowire trigate p-MOSFETs. in *Electron Devices Meeting (IEDM)*, 2012 IEEE International. 2012.
15. Xue Z, et al. "Fabrication of high quality strained SiGe on Si substrate by RPCVD" *Chinese Science Bulletin* May 2012, Volume 57, Issue 15, pp 1862–1867
16. Kim H, et al. Tunneling field-effect transistor with Si/SiGe material for high current drivability. *2014 Jpn J Appl Phys* 53 06JE12
17. Schmidt M, et al. Si/SiGe hetero-structure tunneling field effect transistors with in-situ doped SiGe source. *2012 13th International Conference on Ultimate Integration on Silicon (ULIS)*.
18. Patton GL, et al. Silicon-germanium base heterojunction bipolar transistors by molecular beam epitaxy. *Electron Device Letters, IEEE*, 1988. 9(4): p. 165-167.
19. Patton GL, et al. SiGe-base heterojunction bipolar transistors: physics and design issues. in *Electron Devices Meeting, 1990. IEDM '90. Technical Digest, International. 1990*.

20. Cressler JD, SiGe HBT technology: a new contender for Si-based RF and microwave circuit applications. *Microwave Theory and Techniques, IEEE Transactions on*, 1998. 46(5): p. 572-589.
21. Jae-Sung R, et al. SiGe heterojunction bipolar transistors and circuits toward terahertz communication applications. *Microwave Theory and Techniques, IEEE Transactions on*, 2004. 52(10): p. 2390-2408.
22. Kang Y, Monolithic germanium/silicon avalanche photodiodes with 340 GHz gain–bandwidth product. *Nature Photonics*, 3(1), pp.59-63, 2008.
23. Morse M, Monolithic Ge/Si avalanche photodiodes. *Proc. 6th IEEE Int. Conf. Group IV Photon.* 25–27, 2009.
24. Yin T, et al. 31 GHz Ge n-i-p waveguide photodetectors on silicon-on-insulator substrate. *Opt Express* 15, 13965–13971, 2007.
25. Kuo YH, Lee YK, Ge Y, and Shen R, Strong quantum-confined Stark effect in germanium quantum well structures on silicon. *Nature* 437, 1334–1336, 2005.
26. Roth JE, Fidaner O, Schaevitz RK, Kuo YH, Kamins TI, Harris JS and Miller DA, Optical modulator on silicon employing germanium quantum wells. *Opt. Express* 15, 5851–5859, 2007.
27. Srinivasan S, et al. 56 Gb/s Germanium Waveguide Electro-Absorption Modulator. *Journal of Lightwave Technology*, 34(2), pp.419-424, 2016.
28. Oda K, et al. Fabrication of Ge Waveguides by Epitaxial Lateral Overgrowth toward Monolithic Integration of Light Sources. *ECS Trans* 2016 volume 75, issue 8, 199-209.
29. Oda K, et al. Crystallinity improvements of Ge waveguides fabricated by epitaxial lateral overgrowth. *Japanese Journal of Applied Physics* 55, 04EH06 (2016).
30. Nedeljkovic M, et al. Germanium-on-silicon waveguides operating at mid-infrared wavelengths up to 8.5  $\mu\text{m}$ , *Opt Express* 25, 27431-27441 (2017)
31. Amato M, et al. Silicon–Germanium Nanowires: Chemistry and Physics in Play, from Basic Principles to Advanced Applications, *Chemical Reviews* 2014 114 (2), 1371-1412.
32. Holman Z, Liu CY and Kortshagen U, Germanium and Silicon Nanocrystal Thin-Film Field-Effect Transistors from Solution, *Nano Letters* 2010 10 (7), 2661-2666
33. Dong, Y, et al. "Photoluminescence from Ge-SiO<sub>2</sub> thin films and its mechanism" *Chinese Science Bulletin* August 2001, Volume 46, Issue 15, pp 1268–1271.
34. Grydlik M, et al. Lasing from Glassy Ge Quantum Dots in Crystalline Si. *ACS Photonics*, 2016, 3 (2), pp 298–303.
35. Elkurdi M, et al. "Near-infrared waveguide photodetector with Ge/Si self-assembled quantum dots", *Appl Phys Lett*, vol. 80, no. 3, pp. 509-511, Jan. 2002.
36. Zhang Q, et al. Theoretical analysis of performance enhancement in GeSn/SiGeSn light-emitting diode enabled by Si<sub>3</sub>N<sub>4</sub> liner stressor technique. *Applied Optics* Vol. 55, Issue 34, pp. 9668-9674 (2016).
37. Driesch N, et al. Advanced GeSn/SiGeSn Group IV Heterostructure Lasers. *Adv Sci* 2018, 5, 1700955.
38. Buka D, et al. GeSn lasers for monolithic integration on Si. 2015 IEEE Summer Topicals Meeting Series (SUM).
39. Liu J, et al. Monolithic Ge-on-Si lasers for large-scale electronic–photonic integration. *Semicond Sci Technol* 27 094006.
40. Mathews J, et al. Extended performance GeSn/Si(100) p-i-n photodetectors for full spectral

- range telecommunication applications. APPLIED PHYSICS LETTERS 95, 133506 (2009).
41. Cong H, et al. Silicon Based GeSn p-i-n Photodetector for SWIR Detection. IEEE Photonics Journal (Volume: 8, Issue: 5, Oct. 2016).
  42. Guo D, et al. FINFET Technology Featuring High Mobility SiGe Channel for 10nm and Beyond, IEDM 2016.
  43. Lee CH, et al. A comparative study of strain and Ge content in Si<sub>1-x</sub>Ge<sub>x</sub> channel using planar FETs, FinFETs, and strained relaxed buffer layer FinFETs IEEE 2017.
  44. Huang Y, et al. First Vertically Stacked GeSn Nanowire pGAAFETs with Ion=1850μA/μm (VOV=VDS=-1V) on Si by GeSn/Ge CVD Epitaxial Growth and Optimum Selective Etching, IEDM 2017.
  45. Gupta S, Moroz V, Smith L, Lu Q and Saraswat K, 7-nm FinFET CMOS Design Enabled by Stress Engineering Using Si, Ge, and Sn, in IEEE Transactions on Electron Devices, vol. 61, no. 5, pp. 1222-1230, May 2014.
  46. Yang Y, et al. Towards direct band-to-band tunneling in P-channel tunneling field effect transistor (TFET): Technology enablement by Germanium-tin (GeSn), 2012 International Electron Devices Meeting, San Francisco, CA, 2012, pp. 16.3.1-16.3.4. doi: 10.1109/IEDM.2012.6479053
  47. Heinemann B, et al. SiGe HBT with fx/fmax of 505 GHz/720 GHz. in Electron Devices Meeting, 2017. IEDM'17. International, pp.51-54.
  48. Fahey PM, Griffin PB and Plummer JD, Point defects and dopant diffusion in silicon. Reviews of Modern Physics, 1989. 61(2): p. 289-384.
  49. Liu J, et al. Ge-on-Si laser operating at room temperature. Optics Letters, 2010. 35(5): p. 679-681.
  50. Sun X, et al. A Ge-on-Si laser for electronic-photonics integration. in Lasers and Electro-Optics, 2009 and 2009 Conference on Quantum electronics and Laser Science Conference. CLEO/QELS 2009. Conference on. 2009.
  51. Camacho-Aguilera RE, et al. "An electrically pumped germanium laser," Opt. Express 20, 11316-11320 (2012)
  52. Michel J, et al. An electrically pumped Ge-on-Si laser. in Optical Fiber Communication Conference and Exposition (OFC/NFOEC), 2012 and the National Fiber Optic Engineers Conference. 2012.
  53. Wirths S, Geiger R, et al. Optically pumped GeSn Microdisk Lasers on Si Nat Photonics, vol. 9, pp. 88-92, 2015.
  54. Stange D, Wirths S, Geiger R, et al. Optically Pumped GeSn Microdisk Lasers on Si, ACS Photonics, vol. 3, no. 7, pp. 1279-1285, Jul. 2016.
  55. Al-kabi S, et al. An optically pumped 2.5 μm GeSn laser on Si operating at 110 K, Appl Phys Lett, vol. 109, pp. 171105, 2016.
  56. Personal communications with Dr. Jifeng Liu, 2010.
  57. Sukhdeo DS, et al. Direct bandgap germanium-on-silicon inferred from 5.7% <100>uniaxial tensile strain (Invited), Photonics Res., vol. 2, no. 3, pp. A8 - A13, Jun. 2014.
  58. Cai F, et al. Study of Si-Ge Interdiffusion with Phosphorus Doping, Journal of Applied Physics, vol. 120, 2016, p. 165108.
  59. Castrillo P, et al. Atomistic modeling of defect diffusion and interdiffusion in SiGe heterostructures. Thin Solid Films, 2010. 518(9): p. 2448-2453.

60. Castrillo P, et al. Physical modeling and implementation scheme of native defect diffusion and interdiffusion in SiGe heterostructures for atomistic process simulation. *Journal of Applied Physics*, 2011. 109(10): p. 103502.
61. Zhou G, et al. Impacts of Doping on Epitaxial Germanium Thin Film Quality and Si-Ge Interdiffusion. *Optical Materials Express*, 2018, vol. 8, pp. 1117-1131.
62. Huang B, et al. 10 nm vs 10 nm technology node comparison, Material Science Service Corporation report 2018.
63. Srinivasan S, et al. Extraction of carrier lifetime in Ge waveguides using pump probe spectroscopy. *Applied Physics Letters* 108, 211101 (2016).
64. Malik A, et al. Germanium-on-silicon mid-infrared waveguides and Mach-Zehnder interferometers. 978-1-4577-1507-5/13 2013 IEEE.
65. Gassenq A, et al. GeSn/Ge heterostructure short-wave infrared photodetectors on silicon. *Optics express* Vol. 20, No. 25, 3 December 2012.
66. Tseng C, et al. GeSn waveguide photodetectors fabricated by rapid-melt-growth method. 2015 International Symposium on Next-Generation Electronics.
67. Peng Y, et al. GeSn p-i-n waveguide photodetectors on silicon substrates. *Applied Physics Letters* 105, 231109 (2014).
68. Li Z, et al, Optical Pumped GeSn Waveguides Room Temperature Amplified Spontaneous Emission Observation. ECS meeting abstracts MA2018-02 1034.
69. Zhou Y, et al, Systematic study of GeSn heterostructure-based light-emitting diodes towards mid-infrared applications. *Journal of Applied Physics* 120, 023102 (2016).
70. Dong Y, et al. A unified interdiffusivity model and model verification for tensile and relaxed SiGe interdiffusion over the full germanium content range. *Journal of Applied Physics*, 2012. 111(4): p. 044909.
71. Xia GR, Hoyt JL and Canonico M, Si-Ge interdiffusion in strained Si/strained SiGe heterostructures and implications for enhanced mobility metal-oxide-semiconductor field-effect transistors. *Journal of Applied Physics*, 2007. 101(4): p. 044901.
72. Dong Y, et al. On the role and modeling of compressive strain in Si-Ge interdiffusion for SiGe heterostructures, *Semiconductor Science and Technology*, vol. 29, 2014, pp. 015012
73. Zhou G, et al. Impacts of Doping on Epitaxial Germanium Thin Film Quality and Si-Ge Interdiffusion. *Optical Materials Express*, 2018, vol. 8, pp. 1117-1131.
74. Cowern NEB, et al. DIFFUSION IN STRAINED SI(GE). *Physical Review Letters*, 1994. 72(16): p. 2585-2588.
75. Hollander B, Butz R and Mantl S, INTERDIFFUSION AND THERMALLY INDUCED STRAIN RELAXATION IN STRAINED SI1-XGEX/SI SUPERLATTICES. *Physical Review B*, 1992. 46(11): p. 6975-6981.
76. Iyer SS and Legoues FK, THERMAL RELAXATION OF PSEUDOMORPHIC SI-GE SUPERLATTICES BY ENHANCED DIFFUSION AND DISLOCATION MULTIPLICATION. *Journal of Applied Physics*, 1989. 65(12): p. 4693-4698.
77. Baribeau JM, X-RAY REFLECTOMETRY STUDY OF INTERDIFFUSION IN SI/GE HETEROSTRUCTURES. *Journal of Applied Physics*, 1993. 74(6): p. 3805-3810.
78. Baribeau JM, X-ray scattering analysis of interface roughness and diffusion. *Journal of Vacuum Science & Technology B*, 1998. 16(3): p. 1568-1574.
79. Schorer R, et al. STRUCTURAL STABILITY OF SHORT-PERIOD SI/GE SUPERLATTICES STUDIED

- WITH RAMAN-SPECTROSCOPY. *Physical Review B*, 1991. 44(4): p. 1772-1781.
80. Boucaud P, et al. Photoluminescence and intersubband absorption spectroscopy of interdiffused Si/SiGe quantum wells. *Journal of Applied Physics*, 1996. 80(3): p. 1414-1421.
  81. Aubertine DB and McIntyre PC, Influence of Ge concentration and compressive biaxial stress on interdiffusion in Si-rich SiGe alloy heterostructures. *Journal of Applied Physics*, 2005. 97(1): p. 013531.
  82. Ozguven N and McIntyre PC, Silicon-germanium interdiffusion in high-germanium-content epitaxial heterostructures. *Applied Physics Letters*, 2008. 92(18): p. 181907.
  83. Meduna M, et al. Interdiffusion in SiGe alloys with Ge contents of 25% and 50% studied by X-ray reflectivity. *Physica Status Solidi a-Applications and Materials Science*, 2008. 205(10): p. 2441-2448.
  84. Meduna M, et al. Interdiffusion in Ge rich SiGe/Ge multilayers studied by in situ diffraction. *Physica Status Solidi a-Applications and Materials Science*, 2009. 206(8): p. 1775-1779.
  85. Liu XC and Leadley DR, Silicon-germanium interdiffusion in strained Ge/SiGe multiple quantum well structures. *Journal of Physics D-Applied Physics*, 2010. 43(50): p. 055102.
  86. Gavelle M, et al. Detailed investigation of Ge-Si interdiffusion in the full range of Si<sub>1-x</sub>Ge<sub>x</sub> (0 ≤ x ≤ 1) composition. *Journal of Applied Physics*, 2008. 104(11): p. 113524.
  87. Darken LS, DIFFUSION, MOBILITY AND THEIR INTERRELATION THROUGH FREE ENERGY IN BINARY METALLIC SYSTEMS. *Transactions of the American Institute of Mining and Metallurgical Engineers*, 1948. 175: p. 184-201
  88. McVay GL and Ducharme AR, DIFFUSION OF GE IN SIGE ALLOYS. *Physical Review B*, 1974. 9(2): p. 627-631.
  89. Zangenberg NR, et al. Ge self-diffusion in epitaxial Si<sub>1-x</sub>Ge<sub>x</sub> layers. *Physical Review Letters*, 2001. 87(12): p. 125901.
  90. Strohm A, et al. Self-diffusion of Ge-71 and Si-31 in Si-Ge alloys. *Zeitschrift Fur Metallkunde*, 2002. 93(7): p. 737-744.
  91. Strohm A, et al. Self-diffusion of Ge-71 in Si-Ge. *Physica B-Condensed Matter*, 2001. 308: p. 542-545.
  92. Kube R, et al. Simultaneous diffusion of Si and Ge in isotopically controlled Si<sub>1-x</sub>Ge<sub>x</sub> heterostructures. *Materials Science in Semiconductor Processing*, 2008. 11(5-6): p. 378-383.
  93. Kube R, et al. Composition dependence of Si and Ge diffusion in relaxed Si<sub>1-x</sub>Ge<sub>x</sub> alloys. *Journal of Applied Physics*, 2010. 107(7): p. 073520.
  94. DeHoff R, *Thermodynamics in Materials Science*. 2006, New York: CRC. p232.
  95. Bublik VT, et al. DIFFUSE X-RAY DETERMINATION OF ENERGY OF MIXING AND ELASTIC-CONSTANTS OF GE-SI SOLID-SOLUTIONS. *Physica Status Solidi B-Basic Research*, 1974. 66(2): p. 427-432.
  96. Xia GR, et al. Strain dependence of Si-Ge interdiffusion in epitaxial Si/Si<sub>1-y</sub>Ge<sub>y</sub>/Si heterostructures on relaxed Si<sub>1-x</sub>Ge<sub>x</sub> substrates. *Applied Physics Letters*, 2006. 88(1).
  97. Py M, et al. Characterization and modeling of structural properties of SiGe/Si superlattices upon annealing. *Journal of Applied Physics*, 2011. 110(4): p. 044510.
  98. Guangrui Xia and Judy L. Hoyt, "Si-Ge Interdiffusion under Oxidizing Conditions in Epitaxial SiGe Heterostructures with High Compressive Stress," *Applied Physics Letters*, vol. 96, 2010, pp. 122107-1 to 122107-3.
  99. Cahn JW and Hilliard JE, Free Energy of a Nonuniform System. I. Interfacial Free Energy. *The*

- Journal of Chemical Physics, 1958. 28(2): p. 258-267.
100. Cowern NEB, et al. Interdiffusion Mechanisms in Coherently strained SiGe Multilayers. 1996: p. 195.
  101. Aubertine DB, et al. Observation and modeling of the initial fast interdiffusion regime in Si/SiGe multilayers. Journal of Applied Physics, 2002. 92(9): p. 5027-5035.
  102. Theiss SD, Spaepen F and Aziz MJ, Pressure-enhanced interdiffusion in amorphous Si/Ge multilayers. Applied Physics Letters, 1996. 68(9): p. 1226-1228.
  103. Aziz MJ, Thermodynamics of diffusion under pressure and stress: Relation to point defect mechanisms. Applied Physics Letters, 1997. 70(21): p. 2810-2812.
  104. Ural A, Griffin PB and Plummer JD, Self-Diffusion in Silicon: Similarity between the Properties of Native Point Defects. Physical Review Letters, 1999. 83(17): p. 3454-3457.
  105. Xia G, Dong Y, Si-Ge interdiffusion, dopant diffusion and segregation in SiGe and SiGe: C based devices, Chapter 2, pp. 21-49 in Micro- and Nanoelectronics: Emerging Device Challenges and Solutions, CRC Press, 2015.
  106. Private discussions with Dr. Clement Porrtte and Dr. Andreas Schulze at IMEC.
  107. Schulze A, et al, Non-destructive characterization of extended crystalline defects in confined semiconductor device structures. Nanoscale, 2018, pp.7058-7066.
  108. Fischetti M, and Laux S, Band structure, deformation potentials, and carrier mobility in strained Si, Ge, and SiGe alloys. J. Appl. Phys. 80(4), 2234–2252 (1996).
  109. Ozguven N, and McIntyre P, Oxidation-enhanced interdiffusion in  $\text{Si}_{1-x}\text{Ge}_x$  /  $\text{Si}_{1-y}\text{Ge}_y$  superlattices. Appl. Phys. Lett. 90, 082109, 2007.